Title
Robust Lateral Control of Heavy Duty Vehicles: Final Report

Authors
Tai, Meihua
Tomizuka, Masayoshi

Publication Date
2003-07-01

CALIFORNIA PATH PROGRAM
INSTITUTE OF TRANSPORTATION STUDIES
UNIVERSITY OF CALIFORNIA, BERKELEY

Robust Lateral Control of Heavy Duty Vehicles: Final Report

Meihua Tai, Masayoshi Tomizuka
University of California, Berkeley

California PATH Research Report
UCB-ITS-PRR-2003-24

This work was performed as part of the California PATH Program of the University of California, in cooperation with the State of California Business, Transportation, and Housing Agency, Department of Transportation; and the United States Department of Transportation, Federal Highway Administration.

Final Report for Task Order 4201

July 2003

ISSN 1055-1425

PROJECT TITLE:

Robust Lateral Control of Heavy Duty Vehicles

By

Meihua Tai

Masayoshi Tomizuka

Department of Mechanical Engineering
University of California at Berkeley
Berkeley, CA 94720

Final report for TO 4201

March 2003

Executive Summary

This report summarizes the research results of TO4201, "Robust Lateral Control of Heavy Duty Vehicles." This project represents a continuing effort of PATH's research on Automated Highway Systems (AHS). Research on the lateral control of heavy vehicles for AHS was initiated at PATH in 1993 with MOU129, "Steering and Braking Control of Heavy Duty Vehicles." It was followed by MOU242, "Lateral Control of Commercial Heavy Duty Vehicle," MOU289 (MOU313), "Lateral Control of Heavy Duty Vehicles for Automated Highway Systems," and the current project, MOU385 and TO4201, "Robust Lateral Control of Heavy Duty Vehicles." The earlier projects, MOU129 and MOU242, emphasized theoretical aspects, such as model development, analysis of the dynamic model from the lateral control point of view, and the lateral controller designs. MOU289 (MOU313) focused on the implementation aspects of the lateral controllers: a tractor-semitrailer vehicle was obtained and instrumented with all the necessary hardware and software, open-loop experiments were conducted, system parameters were estimated based on the open-loop tests, and preliminary closed-loop experiments were performed. The current project, MOU385 (TO4201), focuses on designing enhanced robust controllers, experimental validations of the newly designed controllers, and the study of autonomous vehicle following control. TO4201 is a continuation of MOU385, which makes it necessary to comment on the nature of the present report. Results on autonomous lateral control obtained under MOU385 (TO4201), was reported in the final report of MOU385, UCB-ITS-PRR-2001-35, and they are not part of the present report. It is noted that further research on autonomous lateral control is in progress under TO4233, "Fault Tolerant Autonomous Following Lateral Control for Heavy Vehicles." This report summarizes all types of nonlinear and adaptive controllers for lateral control of heavy vehicles and presents an experimental comparative studies of several control algorithms.

Several robust and adaptive controllers are designed to address different aspects of the lane following maneuvers. As a starting point, a sliding mode controller is

designed. The sliding mode controller provides robust stability for systems subject to model uncertainties. However, as the model uncertainty increases, as in the case when both dynamical nonlinear model uncertainty and parametric model uncertainty are present, the performance of the sliding mode controller severely degrades due to the inevitable high control gain. The larger the model uncertainty, the larger the control gain must be set, a consequence of which is the deteriorated control performance. This motivates us to add adaptation to the robust controller to reduce the size of model uncertainty. Such an approach is adaptive robust control (ARC) [33]

The adaptive robust controller provides not only robust stability but also robust performance by taking advantages of both robust controller design technique and adaptive controller design technique while overcoming their shortcomings. The ARC approach is applied to the lateral control of heavy vehicle systems in this research.

Another nonlinear robust controller based on feedback linearization is designed by linearizing the nonlinear lateral vehicle dynamics using a nonlinear state transformation and redefinition of the input to take advantage of the rich linear controller design repertoire. It turns out that the resulting controller resembles the sliding mode controller very closely in appearance. However, they have fundamental differences in achieving robust stability. The two controllers are compared in detail.

The above mentioned sliding mode controller, adaptive robust controller, and nonlinear robust controller based on feedback linearization ignore the dynamics of the steering subsystem. To further improve system performance, the dynamics of the steering subsystem has to be explicitly taken into account in the lateral controller design. In our study, we model the local closed-loop steering subsystem as a first order linear system with model uncertainty. However, the steering subsystem is subject to saturation and rate limit. To account for these realistic aspects of the actuator, we propose a preventive approach, nonlinear loop-shaping. That is, we dynamically extend the vehicle lateral control system, the cascaded connection of the dynamics of the local closed-loop steering subsystem and the vehicle body dynamics, with a low-

pass prefilter, then, design a nonlinear robust controller for the dynamically extended lateral control system. The controller is based on backstepping technique and modified robust control design method base on the Lyapunov theory. The actual input to the steering actuator is the output of the pre-filter. It is proved by simulation that, by explicitly taking into account the steering subsystem dynamics in the lateral controller design, the system performance is greatly improved in terms of the smoothness and magnitude of the input as well as the smoothness of transient responses.

We observe an analogy between the vehicle lateral control system and a mechanical system with a coulomb friction. Motivated by this observation, we propse to use a feedforward compensator to augment the linear robust feedback controllers for reducing lateral tracking errors while sustaining a reasonable passenger comfort. Two feedforward compensators are designed: a fixed-gain feedforward compensator and an adaptive feedforward compensator. Simulation results show that the feedforward compensation effectively reduces the lateral tracking error. Also, by analyzing the contributing terms of the known nonlinearities which are fed back in most of the nonlinear controllers, we found that the known nonlinear terms actually involve a feedforward compensation term corresponding to fixed-gain feedforward compensation. Therefore, it is concluded that a feedforward compensation in addition to a robust linear feedback controller is a mid-point between nonlinear controllers and linear robust controllers in terms of the ease of implementation and the improved control system performance.

The sliding mode controller, a linear robust controller with feedforward compensation, and the same linear robust controller are implemented on a tractor-semitrailer combination and compared experimentally.

Abstract

In this report, achievements under TO4201, "Robust Lateral Control of Heavy Duty Vehicles," are presented. The purposes of this project are: to design new controllers or redesign existing controllers for lateral control of heavy vehicles to improve performance; to evaluate designed controllers by experiments and to study autonomous vehicle following control. TO4201 is a continuation of MOU385, which makes it necessary to comment on the nature of the present report. Results on autonomous lateral control obtained under MOU385 (TO4201), was reported in the final report of MOU385, UCB-ITS-PRR-2001-35, and they are not part of the present report. It is noted that further research on autonomous lateral control is in progress under TO4233, "Fault Tolerant Autonomous Following Lateral Control for Heavy Vehicles." This report summarizes all types of nonlinear and adaptive controllers for lateral control of heavy vehicles and presents an experimental comparative studies of several control algorithms.

The vehicle lateral control model is nonlinear and has two types of model uncertainties: dynamical nonlinear uncertainties and parametric uncertainties. To achieve robust stability as well as robust performance, various nonlinear robust control techniques such as sliding mode control, adaptive robust control, and robust nonlinear control based on feedback linearization are sought. To further improve robust performance, the dynamics of the steering subsystem is considered in the lateral controller design. In doing so, to account for the saturation and rate limit in the steering subsystem, a nonlinear loop-shaping approach is proposed. An analogy between the road disturbance to a vehicle lateral control system and the Coulomb friction to a mechanical system is observed. Based on this observation, two feedforward compensators are proposed which can be used in combination with linear robust controllers to further improve tracking performance of the linear feedback control systems. The sliding mode controller, a linear robust controller with feedforward compensation, and the same linear robust controller are implemented on a tractor-semitrailer combination

and compared experimentally.

Keywords: *Automated Highway Systems, Model uncertainty, Nonlinear control, Robust control, Adaptive control, Backstepping design, Lateral control, Heavy duty vehicles*

1 Introduction

The ever-growing needs of increasing traffic capacity and relieving traffic congestion, coupled with the difficulty and cost ineffectiveness of building new highways, motivated the idea of Intelligent Vehicle-Highway Systems (IVHS). In an Intelligent Vehicle-Highway System, various combinations of advanced technologies such as control, communication, networking, computational technology and information technology are applied to increase traffic throughput and relieve traffic congestion without building new highways. Among the various forms of "intelligence" with the different levels of controls imposed on vehicles and on highway systems, it is argued that only the fully automated highway systems can achieve significant increase of traffic capacity [17, 15, 25, 2, 3, 1, 13, 16, 24, 28]. The fully automated highway systems are called Automated Highway Systems (AHS). The benefits of AHS also include the improved highway safety and fuel economy, and the reduced air pollution.

Although the AHS was studied over half a century, the most extensive and systematic research was conducted from the mid 1980's, and until recently, the focus was on the passenger cars. Research by the Federal Department of Transportation shows that, in the United States, the transportation of goods by heavy trucks climbed from the 20% of all freight transportation in 1970 to the 45% in 1990 and it is expected to grow further. Heavy vehicles usually operate long distance and in groups on preselected routes. These operational characteristics of trucking industry make the AHS concept more attractive for heavy vehicles than for passenger cars. Furthermore, because of the cost effectiveness, multi-unit heavy trucks are gaining more and more attention from trucking industry, and multi-unit commuter buses are under investigation as an option for public transportation [4].

PATH has been conducting research on the lateral control of heavy vehicles in the context of AHS since 1993. The research has covered modeling, linear analysis of the dynamic model, and development of linear and nonlinear control algorithms. Chen and Tomizuka [5] derived a 5 degree-of-freedom (DOF) model for a tractor-

semitrailer vehicle system. Wang and Tomizuka [29] analyzed the linear model of tractor-semitrailer type of vehicles in both time domain and frequency domain and studied the effects of the look-ahead distance, road adhesion coefficients and vehicle velocity on the system dynamics. Based on the linear analysis and open-loop test results, a lead-lag controller was designed and tested [29]. To cope with model uncertainties in the linearized model, a H_∞ loop-shaping controller was designed [30]. As with passenger cars, the vehicle velocity appears in coefficients of heavy vehicle models. Consequently, a gain-scheduling controller with the vehicle velocity as a scheduling paramter [32] and a Liner Parameter Varying (LPV) controller [12] were designed so that the vehicle can be robustly operated over a wide range of velocity. To improve handing property and reduce off-tracking, a coordination between steering and differential braking was also studied [7, 6, 31].

In the lateral control model of a heavy vehicle system, only the translational motion and yaw motion of each unit are considered and the road-tire interaction is modeled as a linear function of tire cornering stiffness. So, the lateral control model (by abuse of terminologies, here and hereafter, we mean the vehicle body dynamics, unless otherwise specified) has unmodeled dynamics such as the roll and pitch motions and their coupling, bouncing motion, suspension dynamics, and nonlinear road-tire interaction. It also has parametric uncertainties such as uncertainties in the vehicle inertial parameters (mass and moment of inertia) and dimensional parameters related to the location of the center of gravities of each unit due to the varying loads on the trailers, and tire cornering stiffness due to the changing road conditions. As in the passenger car, due to the centrifugal and Coriolis force terms, the control model of a heavy vehicle system is nonlinear. Therefore, robust nonlinear control techniques provide a natural candidate for the lateral controller. Compared to the passenger cars, each unit of a heavy vehicle system has a higher center of gravity and more easily rolls over. Multi-unit heavy vehicles have unstable yaw modes such as jackknifing, fishtailing and trailer swinging, and because of the longer length, the off-tracking problem

is more prominent. Considering all of these aspects, the controllers are required not only to be robustly stable under the model uncertainties but also to provide robust performance.

Several controllers are designed to address different aspects of the lane following maneuver. As a starting point, a sliding mode controller is designed. The sliding mode controller provides robust stability for systems subject to model uncertainties. However, as the model uncertainty increases, as in the case when both dynamical nonlinear model uncertainty and parametric model uncertainty are present, the performance of the sliding mode controller severely degrades due to the inevitable high control gain. The larger the model uncertainty, the larger the control gain must be set, a consequence of which is the deteriorated control performance. This motivates us to add adaptation to the robust controller to reduce the size of model uncertainty. Such an approach is adaptive robust control (ARC) [33]

The adaptive robust controller provides not only robust stability but also robust performance by taking advantages of both robust controller design technique and adaptive controller design technique while overcoming their shortcomings. The ARC approach is applied to the lateral control of heavy vehicle systems in this research.

Another nonlinear robust controller based on feedback linearization is designed by linearizing the nonlinear lateral vehicle dynamics using a nonlinear state transformation and redefinition of the input to take advantage of the rich linear controller design repertoire. It turns out that the resulting controller resembles the sliding mode controller very closely in appearance. However, they have fundamental differences in achieving robust stability. The two controllers are compared in detail.

The above mentioned sliding mode controller, adaptive robust controller, and nonlinear robust controller based on feedback linearization ignore the dynamics of the steering subsystem. To further improve system performance, the dynamics of the steering subsystem has to be explicitly taken into account in the lateral controller design. In our study, we model the local closed-loop steering subsystem as a first or-

der linear system with model uncertainty. However, the steering subsystem is subject to saturation and rate limit. To account for these realistic aspects of the actuator, we propose a preventive approach, nonlinear loop-shaping. That is, we dynamically extend the vehicle lateral control system, the cascaded connection of the dynamics of the local closed-loop steering subsystem and the vehicle body dynamics, with a low-pass prefilter, then, design a nonlinear robust controller for the dynamically extended lateral control system. The controller is based on backstepping technique and modified robust control design method base on the Lyapunov theory. The actual input to the steering actuator is the output of the pre-filter. It is proved by simulation that, by explicitly taking into account the steering subsystem dynamics in the lateral controller design, the system performance is greatly improved in terms of the smoothness and magnitude of the input as well as the smoothness of transient responses.

We observe an analogy between the vehicle lateral control system and a mechanical system with a coulomb friction. Motivated by this observation, we propse to use a feedforward compensator to augment the linear robust feedback controllers for reducing lateral tracking errors while sustaining a reasonable passenger comfort. Two feedforward compensators are designed: a fixed-gain feedforward compensator and an adaptive feedforward compensator. Simulation results show that the feedforward compensation effectively reduces the lateral tracking error. Also, by analyzing the contributing terms of the known nonlinearities which are fed back in most of the nonlinear controllers, we found that the known nonlinear terms actually involve a feedforward compensation term corresponding to fixed-gain feedforward compensation. Therefore, it is concluded that a feedforward compensation in addition to a robust linear feedback controller is a mid-point between nonlinear controllers and linear robust controllers in terms of the ease of implementation and the improved control system performance.

The sliding mode controller, a linear robust controller with feedforward compensation, and the same linear robust controller are implemented on a tractor-semitrailer

combination and compared experimentally.

The rest of the report is organized as follows. In the following section, the system output, the lateral tracking error, is formulated. Different aspects of the lateral control of heavy vehicles for AHS are investigated in sections 3-7 and experimental studies are presented in section 8. Section 9 concludes this report.

2 System Model

The complex model used in this research to verify the control algorithms by simulation and the control model with which the model based control algorithms are developed are the ones derived under MOU 289 and documented in California PATH Research Report, UCB-ITS-PRR-98-8. In the simulation model, both tractor and semitrailer are considered as rigid bodies with 6 DOF unless constrained by hitching mechanisms. The coupling of the roll and pitch motions is modeled from the view point of geometry. The control model considers only the translational motion of the system and yaw motions of the tractor and the semitrailer. In this section, we formulate the system output by introducing a road coordinate system and two-sensor scheme.

2.1 Model in vehicle coordinate system

Throughout this report, we assume that only the tractor's front wheels are steerable for the tractor-semitrailer type of heavy vehicles. In the control model of a tractor-semitrailer combination given by Eq. (165) of California PATH Research Report, UCB-ITS-PRR-98-8, denote $N_f^1 C_{\alpha f}^1$ as $C_{\alpha f}$, $N_r^1 C_{\alpha r}^1$ as $C_{\alpha r}$ and $N_r^2 C_{\alpha r}^2$ as $C_{\alpha t}$, and let $N_f^2 = 0$, $\delta_2 = 0$ and $\delta_1 = \delta_f$. By abuse of notation, let $q = (y, \varepsilon_1, \varepsilon_f)^T$, where $\varepsilon_f = \varepsilon_2 - \varepsilon_1$ is the articulation angle and $y(t) = y(0) + \int_0^t V_y(\tau) d\tau$. Then, $\dot{q} = (V_y, \dot{\varepsilon}_f, \dot{\varepsilon}_f)^T$ and Eq. (165) can be rewritten as

$$M(q)\ddot{q} + c(q, \dot{q}, V_x) = 2C_{\alpha f}(1, l_{f1}, 0)^T \delta_f, \tag{1}$$

where the right hand side of the equation represents terms contributed from the linear tire model which are steering angle dependent, M is a 3×3 inertia matrix, and c represents the sum of centrifugal and coriolis forces as well as terms from the linear tire model which are not steering angle dependent. See Appendix A for details. These equations of motion are given in the vehicle coordinate system, the U_1-frame. Due to its formulation, y and ε_1 do not appear in Eq. (1).

Note that, in Eq. (1), the inertia matrix M is a function of the articulation angle ε_f, which shows the coupling between the dynamics of the tractor and that of the semitrailer. The c term is a set of nonlinear functions of q and $\dot{q}$, and, V_x and $\frac{1}{V_x}$ appear as time varying coefficients.

2.2 Road coordinate system

The purpose of the lateral control of a vehicle in Automated Highway Systems is to let the vehicle follow a desired trajectory, the road centerline in the lane following manoeuver and the designed trajectory in the lane changing manoeuver. In this report, we are exclusively interested in the lane following manoeuver. To achieve this automated trajectory tracking, first of all, we need a method of measuring the tracking error. We call it a road reference / sensing system. There are many ways of doing this. For example, a vision based guidance [23], optical marker-laser radar based guidance [19, 21], guided by wire [9, 11], GPS [10] or magnetic marker-on board magnetometer based guidance [20]. PATH adopted a magnetic sensing scheme [35]. That is, we assume that in automated highway systems, all the highways are buried with magnets and all the vehicles are installed with magnetometers which can measure the strength of the magnetic field or the lateral deviation of the vehicle at the sensor location from the road centerline.

To quantify the lateral tracking error, we introduce a road coordinate system as shown in Fig. 1. At every moment, the intersection of the road centerline and the ray which connects the center of the road-curve to the c.g. of the tractor is defined to

be the origin, O_r, and the tangent line of the road-curve at O_r is defined to be the X_r-axis with the positive direction pointing to the vehicle travelling direction. The positive direction of the Y_r-axis is chosen such that positive X_r axis, positive Y_r axis and a vector points upward constitute a right-handed cartesian coordinate system in space. Thus, the road coordinate system, $O_rX_rY_r$, is a co-rotational coordinate system in plane with the rotational rate, denoted by $\dot{\varepsilon}_d$, determined by the geometry of the desired trajectory and the longitudinal velocity of the tractor as

$$\dot{\varepsilon}_d = V_x \rho, \tag{2}$$

where ρ is the curvature of the road-curve at the origin. Then, ε_d has the physical meaning of the inclination angle of the positive X_r axis measured in the inertial coordinate system, the n-frame. Then, the orientation of the tractor in the road coordinate system, ε_r, is given by

$$\varepsilon_r = \varepsilon_1 - \varepsilon_d. \tag{3}$$

Let $\mathbf{i_r}$ and $\mathbf{j_r}$ be two unit vectors in the directions of the positive X_r-axis and the positive Y_r-axis, respectively. Then,

$$\frac{d}{dt}\mathbf{i_r} = \dot{\varepsilon}_d \mathbf{j_r} \qquad \text{and} \qquad \frac{d}{dt}\mathbf{j_r} = -\dot{\varepsilon}_d \mathbf{i_r}. \tag{4}$$

Let (x_r, y_r) be the coordinate of the c.g. of the tractor in the road coordinate system. Then, the position vector of the c.g. of the tractor, $\mathbf{r}$, is

$$\mathbf{r} = \mathbf{O_r} + x_r \mathbf{i_r} + y_r \mathbf{j_r} \tag{5}$$

where $\mathbf{O}_r$ represents the position vector of the origin, O_r, of the road coordinate system in the inertial coordinate system. Then, the velocity of the c.g. of the tractor is given by

$$\begin{aligned} \mathbf{V_{c.g.}} = \frac{d}{dt}\mathbf{r} &= \frac{d}{dt}\mathbf{O_r} + \dot{x}_r \mathbf{i_r} + x_r \frac{d}{dt}\mathbf{i_r} + \dot{y}_r \mathbf{j_r} + y_r \frac{d}{dt}\mathbf{j_r} \\ &= \frac{d}{dt}\mathbf{O_r} + (\dot{x}_r - \dot{\varepsilon}_d y_r)\mathbf{i_r} + (\dot{y}_r + \dot{\varepsilon}_d x_r)\mathbf{j_r}. \end{aligned} \tag{6}$$

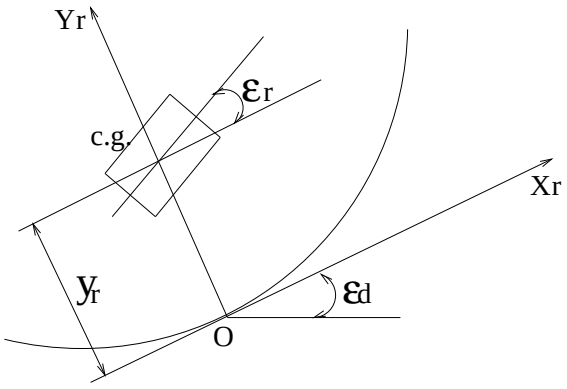

Figure 1: Road Reference Coordinate System

From the definition of the road coordinate system,

$$x_r = 0, \tag{7}$$

and

$$\frac{d}{dt}\mathbf{O_r} = (*)\mathbf{i_r}. \tag{8}$$

On the other hand,

$$\mathbf{V_{c.g.}} = (V_x - \varepsilon_r V_y)\mathbf{i_r} + (V_y + \varepsilon_r V_x)\mathbf{j_r} \tag{9}$$

for a small ε_r. By comparing the $\mathbf{j_r}$ components of Eqs. (6) and (9), and utilizing the facts given by Eqs. (8) and (7), we get

$$\dot{y}_r = V_y + \varepsilon_r V_x. \tag{10}$$

This relation will be used later in formulating the dynamics of the system output.

2.3 Two-sensor scheme and a look-ahead distance

When formulating the system output, we tried to mimic a human driver. When we drive, we do not look down to see where the vehicle is on the road, instead, we look in the front. This can be formulated as the lateral deviation of a point in front of the vehicle from the road centerline. Or, it can be thought of the output of an imaginary magnetometer sensor located in front of the vehicle. The imaginary magnetometer

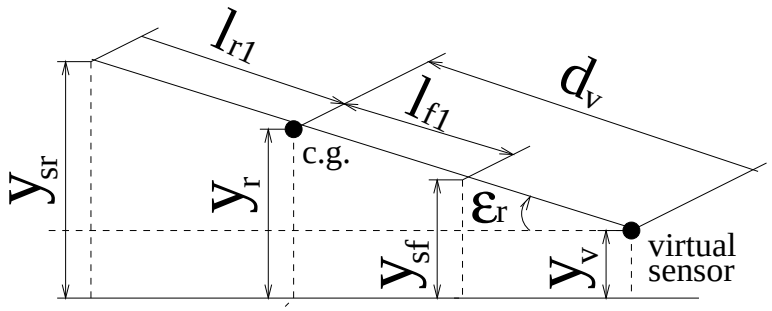

Figure 2: Two Sensor Scheme

is called a *virtual sensor* and the distance of the virtual sensor from the center of gravity of the tractor is called a *look-ahead distance*. By utilizing two-sensor scheme, literally, any look ahead distance can be realized. That is, if we have two lateral error measurements, the lateral deviation, y_s, at any look-ahead distance, d_s, can be calculated by

$$y_s = y_r + d_s \varepsilon_r, \tag{11}$$

where the lateral deviation of the center of gravity of the tractor from the road centerline, y_r, and the yaw angle of the tractor in the road coordinate system, ε_r, are determined from the geometry (cf. Fig. 2) as follows:

$$y_r = \frac{l_{r1} y_{sf} + l_{f1} y_{sr}}{l_{f1} + l_{r1}} \tag{12}$$

and

$$\varepsilon_r = \tan^{-1} \frac{y_{sf} - y_{sr}}{l_{f1} + l_{r1}} \approx \frac{y_{sf} - y_{sr}}{l_{f1} + l_{r1}}, \tag{13}$$

where the approximation holds when ε_r is small.

Note that, in formulating the system output, y_s, we ignore the effect of the road curvature. The US highways consist of series of curved sections and straight sections and the recommended minimum radii for freeways are 5000 feet in rural areas and 3000 feet in urban areas (Highway Design Manual). So, the road curvature is very small, and if the look-ahead distance is not too large, the effect of the road curvature can be ignored. Also note that, in order to keep the tractor's c.g. follow the road

centerline, the virtual sensor should follow a trajectory, y_{sd}, which is different from the road centerline.

Some analytical studies show that the larger the look-ahead distance the easier the control problem becomes in the sense of the increased damping, etc. [29, 22]. We will show later that the look-ahead distance can not be taken arbitrarily large.

3 Sliding Mode Control

As an initial effort, we designed a sliding mode controller, which will serve as a starting point and as motivation for other lateral controllers that will be presented in this report.

3.1 Model reformulation

By differentiating the system output given by Eq. (11), we get

$$\dot{y}_s = \dot{y}_r + d_s\dot{\varepsilon}_r, \tag{14}$$

and by substituting $\dot{y}_r$ in Eq. (14) with Eq. (10), we have

$$\dot{y}_s = V_y + \varepsilon_r V_x + d_s\dot{\varepsilon}_r. \tag{15}$$

The highway roads in the United States are a series of connections of straight sections and arcs of constant radii. Thus, under the assumption that the longitudinal velocity V_x is constant, the desired yaw rate, $\dot{\varepsilon}_d$, is constant on each road segment and $\ddot{\varepsilon}_d$ is zero except at discrete connecting points of different segments of roads. So, the second derivative of y_s is

$$\ddot{y}_s = \dot{V}_y + d_s\ddot{\varepsilon}_1 + V_x\dot{\varepsilon}_r. \tag{16}$$

Remember that Eq. (1) is a set of 3 second order differential equations. By substituting $\ddot{\varepsilon}_f$ obtained from the third equation into the first and second equations, we

have

$$A \begin{pmatrix} \dot{V}_y \\ \ddot{\varepsilon}_1 \end{pmatrix} + b = 2C_{\alpha f} \begin{pmatrix} 1 \\ l_{f1} \end{pmatrix} \delta_f, \tag{17}$$

where

$$\begin{aligned} A &= \begin{pmatrix} M_{11} - \frac{M_{13}}{M_{33}} M_{31} & M_{12} - \frac{M_{13}}{M_{33}} M_{32} \\ M_{21} - \frac{M_{23}}{M_{33}} M_{31} & M_{22} - \frac{M_{23}}{M_{33}} M_{32} \end{pmatrix}, \\ b &= \begin{pmatrix} c_1 - \frac{M_{13}}{M_{33}} c_3 \\ c_2 - \frac{M_{23}}{M_{33}} c_3 \end{pmatrix}, \end{aligned} \tag{18}$$

and M_{ij}-s are the (i, j) elements of M. Let $F = A^{-1}$. Then,

$$\begin{aligned} \dot{V}_y &= F_{11}(2C_{\alpha f}\delta_f - b_1) + F_{12}(2C_{\alpha f} l_{f1}\delta_f - b_2), \\ \ddot{\varepsilon}_1 &= F_{21}(2C_{\alpha f}\delta_f - b_1) + F_{22}(2C_{\alpha f} l_{f1}\delta_f - b_2), \end{aligned} \tag{19}$$

where F_{ij}-s are the (i, j)-elements of F. By substituting Eq. (19) to Eq. (16), the output dynamics becomes

$$\ddot{y}_s = b_0(q, \dot{q})\delta_f + f_0(q, \dot{q}) + \tilde{f}_2(q, \dot{q}), \tag{20}$$

where

$$\begin{aligned} b_0(q, \dot{q}) &= 2C_{\alpha f}\left((F_{11} + d_s F_{21}) + (F_{12} + d_s F_{22}) l_{f1}\right), \\ f_0(q, \dot{q}) &= -\left((F_{11} + d_s F_{21}) b_1 + (F_{12} + d_s F_{22}) b_2\right) + V_x \dot{\varepsilon}_r \end{aligned} \tag{21}$$

and $\tilde{f}_2(q, \dot{q})$ is added to represent the model uncertainties including both unmodeled dynamics and parametric uncertainties.

In summary, the control model for a tractor-semitrailer system is given by

$$\begin{aligned} \dot{x} &= b_{x0}(x)\delta_f + f_{x0}(x) + \tilde{f}_{x2}(x), \\ \ddot{y}_s &= b_0(x)\delta_f + f_0(x) + \tilde{f}_2(x), \end{aligned} \tag{22}$$

where $x = (q^T, \dot{q}^T)^T$ and the first equation is from Eq. (1). The $\tilde{f}_{x2}(x)$ term in the first equation represents the model uncertainties.

Considering the physical properties of the system, we make the following assumptions.

Assumption 1 *The unknown nonlinear functions,* $\tilde{f}_{x2}(x)$ *and* $\tilde{f}_2(x)$*, are bounded above by known functions,* $\beta_x(x)$ *and* $\beta(x)$*, respectively, i.e.,* $\|\tilde{f}_{x2}(x)\| \leq \beta_x(x)$ *and* $\|\tilde{f}_2(x)\| \leq \beta(x)$.

Assumption 2 $b_{x0}(x)$ *and* $b_0(x)$ *are positive functions.*

Note that the first assumption is about the extent of the model uncertainties and the second assumption is to ensure that the input gains are nonzero all the time.

3.2 Controller design

The vehicle output dynamics described by the second equation of Eq. (22) has relative degree of two with respect to the given input-output pair, δ_f and y_s. Define the sliding surface, S, be a stable first order dynamics in terms of the tracking error, e. That is,

$$S = \dot{e} + \lambda e, \tag{23}$$

where λ is a positive parameter. The tracking error is defined as

$$e = y_s - y_{sd}, \tag{24}$$

where y_{sd} is the desired trajectory described in the road coordinate system. Then, the time derivative of S along the system trajectory is

$$\begin{aligned} \dot{S} &= \ddot{e} + \lambda\dot{e} \\ &= \ddot{y}_s - \ddot{y}_{sd} + \lambda\dot{e} \\ &= b_0(x)\delta_f + f_0(x) + \tilde{f}_2(x) - \ddot{y}_{sd} + \lambda\dot{e}. \end{aligned} \tag{25}$$

Choose the control input, δ_f, as

$$\delta_f(x) = -\frac{1}{b_0(x)}\left(f_0(x) - \ddot{y}_{sd} + \lambda\dot{e} + (\beta(x) + k)\mathrm{sgn}(S)\right) \tag{26}$$

where k is a positive design parameter, and sgn is a sign function defined as

$$\mathrm{sgn}(S) = \begin{cases} 1, & S > 0 \\ 0, & S = 0 \\ -1, & S < 0 \end{cases}. \tag{27}$$

Noting Assumption 1, Eqs. (25) and (26) imply

$$\begin{aligned} S\dot{S} &= S\tilde{f}_2(x) - \beta(x)\,|S| - k\,|S| \\ &\leq -k\,|S|\,, \end{aligned} \tag{28}$$

which forces the sliding surface, S, to go to zero within a finite time, $S(t=0)/k$. Since Eq. (23) defines a stable system for $S=0$, the output tracking error will then asymptotically go to zero. One undesired problem of this kind of discontinuous control law is the chattering caused by the sign function. Chattering can be eliminated by substituting the sign function with the continuous saturation function with a prescribed boundary layer, $\phi > 0$. The saturation function, *sat* is defined as

$$\text{sat}\,(S/\phi) = \begin{cases} 1, & S \geq \phi \\ S/\phi, & -\phi \leq S \leq \phi \\ -1 & S \leq -\phi \end{cases} . \tag{29}$$

The modified control law guarantees that the sliding surface reach the boundary of the stable manifold defined by $S=0$ within a finite time.

3.3 Simulation scenario

For the simulation results of the sliding mode controller, adaptive robust controller and linear robust feedback controller with feedforward compensation, the simulation scenarios are the same. Simulation Scenario is described by the desired trajectory and the longitudinal velocity profile. The desired trajectory is as shown in Fig. 3. It is the same as the actual test track in Crows Landing, a small town $90miles$ south of Berkeley. The test track consists of three curved sections extended by two straight sections. The radii of the curved sections are $800m$. The longitudinal velocity profile is as given in the upper plot of Fig. 4. It is taken from one of the experiments conduced at Crows Landing. During experiments, the longitudinal velocity is controlled by the driver. Given the desired trajectory and the velocity profile, the desired yaw rate, $\dot{\varepsilon}_d$, can be obtained by Eq. (2), and it is shown in the lower plot of Fig. 4.

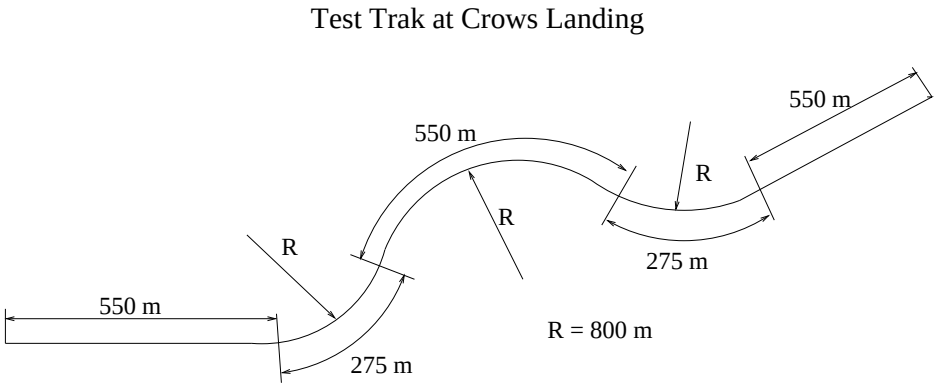

Figure 3: Desired Trajectory/Test Track at Crows Landing

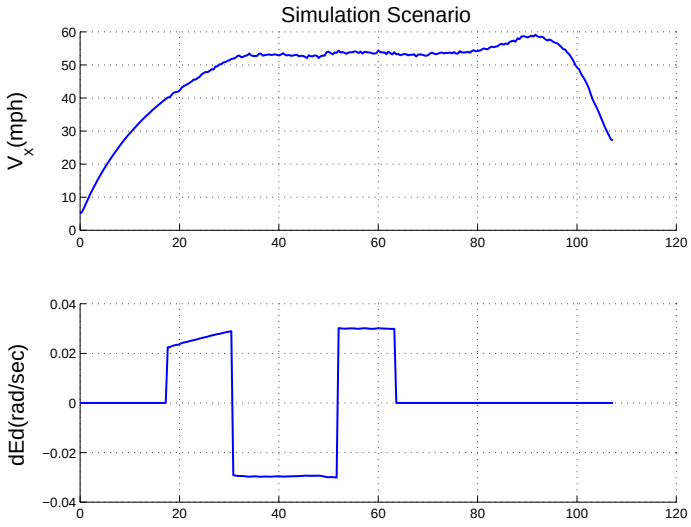

Figure 4: Simulation Scenario

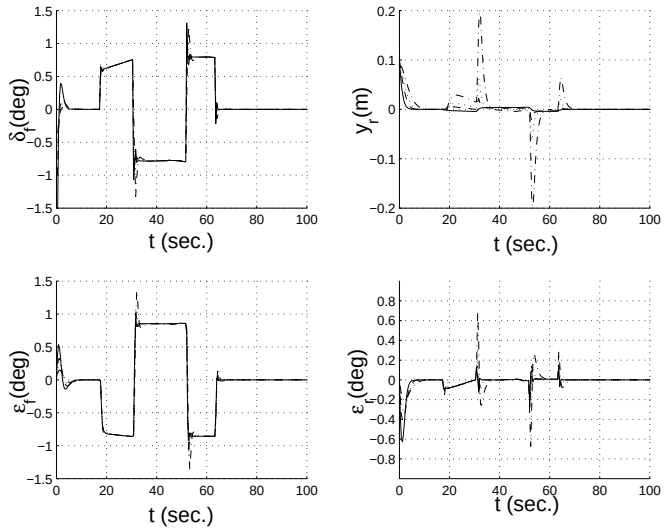

Figure 5: Simulation Result of Sliding Mode Controller for Varying d_s: Solid: $d_s = 0.0m$, Dashed: $d_s = 3.5m$, Dotted: $d_s = 7.0m$, Dash-Dot: $d_s = 15.0m$

3.4 Simulation results

Figures 5 and 6 are the simulation results of the sliding mode controller when the control model is subject to various model uncertainties. They both show that the sliding mode controller robustly stabilizes the lateral dynamics of a tractor-semitrailer system.

Figure 5 shows the simulation results for various look-ahead distance in the case that the control model has only the unmodelled dynamics and the system parameters are assumed to be perfectly known. By increasing the look-ahead distance, the peak steering angle is reduced, tractor yaw rate, articulation angle, tractor yaw error and steering input become smoother. On the other hand, with the increase of the look-ahead distance, the lateral error at tractor's c.g. is increased. This means, with only one control input (steering angle), we have to select look-ahead distance which compromises between the lateral tracking error and the performance. Thus, the look-ahead distance can not be taken too large.

When the control model has parametric uncertainties in addition to the unmodeled

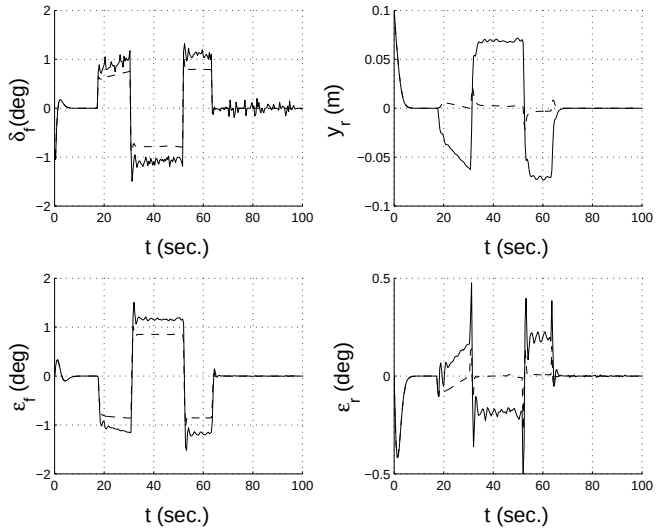

Figure 6: Simulation Results of Sliding Mode Controller: Dashed: No Parametric Uncertainties, Solid: 30% of Parametric Uncertainties in Tire Cornering Stiffness, $C_{\alpha f}$, $C_{\alpha r}$ and $C_{\alpha t}$

dynamics, the model uncertainties are increased, i.e., $\beta(x)$ takes larger values than in the previous case. From Fig. 6, we can see that, with the increase of the model uncertainties, the system performance is dramatically degraded: the steering input becomes larger and has oscillations, the lateral error at the tractor's c.g. and yaw error become larger.

In order to reduce the tracking error, we can increase the control gain, i.e., we can pick a larger k in Eq. (26). This will inevitably result in even higher a gain controller and worsen the control performance even further. It's obvious that the larger the model uncertainty, the higher the gain is expected to obtain the same level of tracking error. This motivates adaptive robust control, which is the topic of the next section.

4 Adaptive Robust Control

In the control model of a tractor-semitrailer system, there exist two types of model uncertainties: unmodeled nonlinear dynamical uncertainties and parametric uncertainties. In the robust controllers such as a sliding mode controller, the two types of model uncertainties are treated in the same manner, that is, they are lumped together and overpowered by a robust term such as a sign function or a saturation function to achieve robust stability. The observations in the previous section suggests that the smaller the uncertainties, the smaller the coefficients of the sign or saturation functions, resulting in a smaller and smoother control inputs. Simulation results in the previous section indicate that additional parametric uncertainties in the tire cornering stiffness, $C_{\alpha f}$, $C_{\alpha r}$, and $C_{\alpha t}$, significantly degrade the performance of the sliding mode controller.

To overcome the high gain nature of robust controllers, we resort to the adaptive control technique and combine it with the robust control techniques. By combining a robust control and an adaptive control in one controller, we, instead of letting the robust controller to deal with both unmodeled dynamics and parametric uncertainties, split the task between the robust controller and the adaptive controller such that the adaptive controller takes care of the parametric uncertainties and the robust controller takes care of the unmodeled dynamics. Thus, we can get a reduced uncertainty bound which the robust controller "sees."

In combining the two control techniques, first of all, we would like to have some control over the transient performance. The transient performance of an adaptive control is not clear and in the presence of dynamical uncertainties, such as unmodeled dynamics and external disturbances, adaptive control systems may become unstable unless robustness is explicitly taken into account. In contrast to the adaptive control, transient performance and final tracking accuracy are guaranteed in a robust control for both parametric uncertainties and dynamical model uncertainties. So, we choose a robust controller as the baseline controller to guarantee the transient performance

and the final tracking error and on top of that, introduce an adaptive controller to reduce the model uncertainty bound for the robust controller to overcome. Yet, the robust controller requires that all the model uncertainties are bounded. However, the traditional adaptation law does not guarantee the boundedness of the parameter estimation error. To successfully incorporate the adaptation technique in the robust controller, the traditional adaptation law is modified by projection method [27, 34] to ensure the boundedness of the estimation error, therefore, the boundedness of the total system model uncertainties. The resulting controller is called the Adaptive Robust Contoller (ARC) [33]. It effectively combines the design methodologies of robust control and adaptive control to keep the advantages of both the robust control and adaptive control while overcoming their drawbacks.

In this section, the ARC method is applied to solve the robust control problem of the vehicle lateral dynamics.

4.1 Model reformulation

To apply adaptive robust control technique to the design of a lateral controller for a tractor-semitrailer system, we decompose the uncertainty terms in Eq. (22) into unmodeled dynamical uncertainties and parametric uncertainties. In our example, the uncertain parameter, θ, is taken to be the tire cornering stiffness, i.e., $\theta = (C_{\alpha f}, C_{\alpha r}, C_{\alpha t})^T$, where $C_{\alpha f}$, $C_{\alpha r}$ and $C_{\alpha t}$ are tractor front tire cornering stiffness, tractor rear tire cornering stiffness and semitrailer tire cornering stiffness, respectively. Then, b in Eq. (17) becomes

$$b = g + h\theta, \tag{30}$$

where

$$
\begin{aligned}
g = \begin{pmatrix} g_1 \\ g_2 \end{pmatrix} &= \begin{pmatrix} k_1 - \frac{M_{13}}{M_{33}} k_3 \\ k_2 - \frac{M_{23}}{M_{33}} k_3 \end{pmatrix}, \qquad \text{with} \\
k_1 &= (m_1 + m_2) V_x \dot{\varepsilon}_1 + m_2 d_{f2} (\dot{\varepsilon}_1 + \dot{\varepsilon}_f)^2 \sin \varepsilon_f, \\
k_2 &= -m_2 (d_{r1} + d_{f2} \cos \varepsilon_f) V_x \dot{\varepsilon}_1 - m_2 d_{f2} V_y \dot{\varepsilon}_1 \sin \varepsilon_f \\
&\quad - 2 m_2 d_{r1} d_{f2} \dot{\varepsilon}_1 \dot{\varepsilon}_f \sin \varepsilon_f - m_2 d_{r1} d_{f2} \dot{\varepsilon}_1^2 \sin \varepsilon_f, \\
k_3 &= -m_2 d_{f2} V_x \dot{\varepsilon}_1 \cos \varepsilon_f - m_2 d_{f2} V_y \dot{\varepsilon}_1 \sin \varepsilon_f + m_2 d_{r1} d_{f2} \dot{\varepsilon}_1^2 \sin \varepsilon_f,
\end{aligned}
\tag{31}
$$

and

$$
\begin{aligned}
h = \begin{pmatrix} h_1 \\ h_2 \end{pmatrix}, &\qquad \text{with} \\
h_1 = &\begin{pmatrix} \frac{2}{V_x} \left(V_y + l_{f1} \dot{\varepsilon}_1 \right) \\ \frac{2}{V_x} \left(V_y - l_{r1} \dot{\varepsilon}_1 \right) \\ \frac{2}{V_x} \left[V_y - \left(d_{r1} + d_{f2} + l_{r2} \right) \dot{\varepsilon}_1 - \left(d_{f2} + l_{r2} \right) \dot{\varepsilon}_f \right] - 2\varepsilon_f - \frac{M_{13}}{M_{33}} \chi \end{pmatrix}^T, \\
h_2 = &\begin{pmatrix} \frac{2}{V_x} \left(V_y l_{f1} + l_{f1}^2 \dot{\varepsilon}_1 \right) \\ \frac{2}{V_x} \left(-V_y l_{r1} + l_{r1}^2 \dot{\varepsilon}_1 \right) \\ \frac{2}{V_x} \left[-V_y l + l^2 \dot{\varepsilon}_1 + \left(d_{f2} + l_{r2} \right) l \dot{\varepsilon}_f \right] + 2 l \varepsilon_f - \frac{M_{13}}{M_{33}} \chi \end{pmatrix}^T, \\
l = &\left(d_{r1} + d_{f2} + l_{r2} \right), \\
\chi = &\frac{2}{V_x} \left[-V_y \left(d_{f2} + l_{r2} \right) + l \left(d_{f2} + l_{r2} \right) \dot{\varepsilon}_1 + \left(d_{f2} + l_{r2} \right)^2 \dot{\varepsilon}_f \right] + 2 \left(d_{f2} + l_{r2} \right) \varepsilon_f.
\end{aligned}
\tag{32}
$$

By substituting Eqs. (19) and (30) to Eq. (16), we have output dynamics in terms of uncertain parameters as follows:

$$
\ddot{y}_s = (b_{y0} + b_{y1}(x)\theta)\delta_f + f_{y0}(x) + f_{y1}(x)\theta + \tilde{f}_{y2}(x), \tag{33}
$$

where

$$
\begin{aligned}
&b_{y0}(x) = 0, \\
&b_{y1}(x) = \left[\begin{array}{ccc} 2\left(F_{11} + d_s F_{21}\right) + 2\left(F_{12} + d_s F_{22}\right) l_{f1} & 0 & 0 \end{array} \right], \\
&f_{y0}(x) = V_x \dot{\varepsilon}_r - \left(F_{11} + d_s F_{21}\right) g_1 - \left(F_{12} + d_s F_{22}\right) l_{f1} g_2, \\
&f_{y1}(x) = -\left(F_{11} + d_s F_{21}\right) h_1 - \left(F_{12} + d_s F_{22}\right) l_{f1} h_2,
\end{aligned}
\tag{34}
$$

with $\tilde{f}_{y2}(x)$ representing the unmodeled dynamical uncertainties in the output dynamics.

In summary, the adaptive robust control model of a tractor-semitrailer system is

$$
\begin{aligned}
&\dot{x} = \left(b_{xy0} + b_{xy1}(x)\theta\right)\delta_f + f_{xy0}(x) + f_{xy1}\theta + \tilde{f}_{xy2}(x), \\
&\ddot{y}_s = \left(b_{y0} + b_{y1}(x)\theta\right)\delta_f + f_{y0}(x) + f_{y1}\theta + \tilde{f}_{y2}(x),
\end{aligned}
\tag{35}
$$

where the first equation is from Eq. (1). The $\tilde{f}_{x2}(x)$ term in the first equation represents the unmodeled dynamical uncertainties. Comparing with the sliding mode control model given in Eq. (22), we have

$$
\begin{aligned}
&b_{x0}(x) = b_{xy0}(x) + b_{xy1}(x)\theta, \\
&f_{x0}(x) = f_{xy0}, \\
&\tilde{f}_{x2}(x) = f_{xy1}(x)\theta + \tilde{f}_{xy2}(x), \\
&b_0(x) = b_{y0}(x) + b_{y1}(x)\theta, \\
&f_0(x) = f_{y0}(x), \\
&\tilde{f}_2(x) = f_{y1}(x) + \tilde{f}_{y2}(x).
\end{aligned}
\tag{36}
$$

Considering the physical properties of a heavy vehicle system, we make the following assumptions.

Assumption 3 *The unknown nonlinear functions, $\tilde{f}_{xy2}(x)$ and $\tilde{f}_{y2}(x)$, are bounded above by known functions, $\beta_{xy}(x)$ and $\beta_y(x)$, respectively, i.e., $\|\tilde{f}_{xy2}(x)\| \leq \beta_{xy}(x)$ and $\|\tilde{f}_{y2}(x)\| \leq \beta_y(x)$.*

Assumption 4 *$b_{xy0}(x) + b_{xy1}(x)(\theta_M - \theta_m)$ and $b_{y0}(x) + b_{y1}(x)(\theta_M - \theta_m)$ are positive functions, where θ_M and θ_m are prescribed upper and lower bound vectors of the uncertain parameter θ.*

Note that the first assumption gives bounds for the model uncertainties and the second assumption guarantees that the input gains are nonzero all the time.

4.2 Controller design

The ARC design utilizes both the proper control structure and the parameter adaptation to reduce the tracking error. The way to accomplish it is to use robust control techniques such as SMC to design a baseline controller (proper control structure) to guarantee transient performance and prescribed final tracking accuracy for both parametric uncertainties and uncertain nonlinearities, and add adaptive control on top of it to update the parameter estimates on-line to reduce the model uncertainties that the robust controller "sees". To do so, one has to solve the conflicts between the two design methodologies. Robust control assumes that model uncertainties are bounded, but the parameters estimated by adaptive control may not be bounded in the presence of unknown nonlinear functions. Thus, one has to modify the conventional parameter adaptation law in such a way that it guarantees that the estimated parameters stay in a prescribed range all the time even in the presence of unknown nonlinear functions. Such a modification should not damage the correct estimation process for parametric uncertainties. In [33], it is achieved by generalizing the smooth projection used in [27]. Here, since the system under consideration does not require any backstepping design, the following simple discontinuous projection method can be used. Suppose ν is the calculated parameter update law, $\dot{\hat{\theta}}$, then, the projection mapping is defined as

$$\text{proj}_{\hat{\theta}}(\nu) = \begin{cases} 0 & \text{when} \quad \hat{\theta} = \theta_M \quad \text{and} \quad \nu > 0 \\ 0 & \text{when} \quad \hat{\theta} = \theta_m \quad \text{and} \quad \nu < 0 \\ \nu & \text{otherwise} \end{cases} . \tag{37}$$

It is shown in [34] that the above robust adaptation law guarantees that $\hat{\theta}$ always stays within the bound defined by θ_M and θ_m, and $\tilde{\theta}\,(proj_{\hat{\theta}}(\nu) - \nu) < 0$ for all ν, where $\tilde{\theta} = \hat{\theta} - \theta$.

We use the same sliding variable as in section 3. Define a scalar Lyapunov function V as

$$V = \frac{1}{2}S^2 + \frac{1}{2\Gamma}\tilde{\theta}^2. \tag{38}$$

Then, the time derivative of V along the system trajectory is

$$\begin{aligned}\dot{V} &= S\dot{S} + \frac{1}{\Gamma}\tilde{\theta}\dot{\hat{\theta}} \\ &= S\left((b_{y0}(x) + b_{y1}(x)\hat{\theta})\delta_f + f_{y0}(x) + f_{y1}(x)\hat{\theta} + \tilde{f}_{y2}(x) + \lambda\dot{e}\right) \\ &\quad + \tilde{\theta}\left(\frac{1}{\Gamma}\dot{\hat{\theta}} - S\left(b_{y1}(x)\delta_f + f_{y1}(x)\right)\right).\end{aligned} \tag{39}$$

Choose the control law for δ_f as

$$\delta_f = -\frac{1}{(b_{y0} + b_{y1}\hat{\theta})}\left(f_{y0} + f_{y1}\hat{\theta} + \lambda\dot{e} + \frac{\beta_{y1}^2 S}{4\epsilon} + kS\right), \tag{40}$$

where $\epsilon > 0$ and $k > 0$ are design parameters, and choose the adaptation law as

$$\dot{\hat{\theta}} = \mathrm{proj}_{\hat{\theta}}\left(\Gamma S(b_{y1}\delta_f + f_{y1})\right). \tag{41}$$

Then, $\dot{V} \leq \epsilon - kS^2 = \epsilon - 2kV$. This implies that V will exponentially converge to a region whose size can be made arbitrarily small, which in turn means the convergence of the output tracking error to an arbitrarily small region.

4.3 Simulation results

In Fig. 7, the solid lines show the simulation results of the sliding mode controller designed in the previous section when, in addition to the unmodeled dynamics, there is 30% of parametric uncertainties, and the dashed lines show the simulation results of the adaptive robust controller under the same conditions. In both cases, the look-ahead distance is chosen to be $d_s = 3.5m$. Apparently, the ARC achieves not only good tracking but also better transient performances with a much smoother steering input than the SMC.

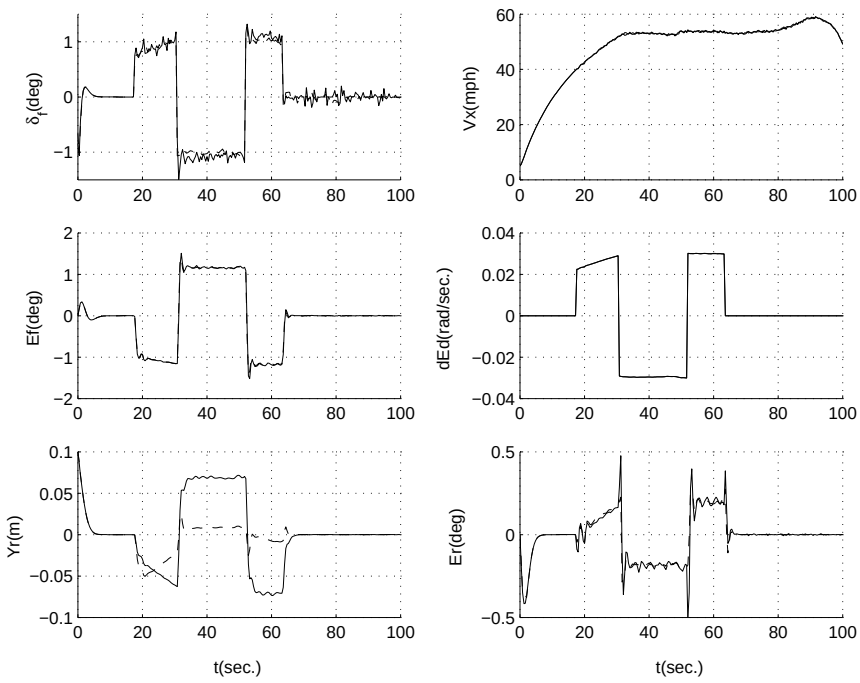

Figure 7: Simulation Results: Dashed:ARC, Solid:SMC

5 Robust Feedback Linearization Control

Other than direct linearization about an operating point, feedback linearization can also convert a nonlinear system to a linear system. When the nonlinear system dynamics are exactly known and the relative degree is definite, there exists a nonlinear state transformation and an input redefinition which transforms the original nonlinear system to a linear system in the new coordinate system [14]. This enables us to take advantage of linear controller design method without sacrificing the accurate representation of system dynamics. In feedback linearization, it is assumed that the exact model of the nonlinear system is known, which is very hard to be satisfied. Nonetheless, the uncertain tractor-semitrailer model in the road coordinate system assumes a canonical form enabling the nonlinear uncertain model be transformed to a linear model with uncertainties. It is noted that the standard SMC implicitly uses feedback linearization.

In this section, we explore the use of feedback linearization in the design of two closely related but different nonlinear robust controllers for lateral guidance of tractor-semitrailer vehicles. One design resembles the ultimate bounded control approach originally proposed by [8]. The other is based on sliding mode control. The basic philosophy behind the use of nonlinear robust control is to build robustness into the control algorithm. The controllers rendered above are designed to robustly maintain small lateral tracking error. The other control objective, passenger comfort, is not directly addressed in controller design, and it must be checked and the controllers be fine tuned by simulations and experiments. Thus, in this section, we will also examine implementation issues of nonlinear controllers.

5.1 Controller design

The dynamics of a tractor-semitrailer system described by Eq. (22) is nonlinear and has model uncertainties. Thus, it violates the assumption of the traditional feedback linearization method which assumes an exact knowledge of the system dynamics. However, the system model satisfies matching conditions, i.e., the control action and uncertainties are in the same channel. Therefore, if we let

$$\delta_f = \frac{1}{b_0(x)}(-f_0(x) + v), \tag{42}$$

then, the system output dynamics becomes

$$\ddot{y}_s = v + \tilde{f}_2(x, \dot{\epsilon}_d). \tag{43}$$

The resulting system is a second order linear system with an uncertainty term. By further letting $y = [y_s, \dot{y}_s]^T$, we have

$$\dot{y} = Ay + Bv + B\tilde{f}_2(x, \dot{\varepsilon}_d), \tag{44}$$

where,

$$A = \begin{bmatrix} 0 & 1 \\ 0 & 0 \end{bmatrix}, \qquad B = \begin{bmatrix} 0 \\ 1 \end{bmatrix}. \tag{45}$$

Note that the pair (A, B) is controllable. If there is no model uncertainty, i.e. $\tilde{f}_2(x, \dot{\varepsilon}_d) = 0$, then there exits a stabilizing state feedback controller, $v = -Ky$, where K is chosen such that $A - BK$ has eigenvalues with negative real parts. To deal with the uncertainty term, we use the robust control law

$$v = -Ky - W, \tag{46}$$

where W is a scalar to be designed. Then,

$$\dot{y} = (A - BK)y + B\tilde{f}_2(x, \dot{\epsilon}_d) - BW. \tag{47}$$

Let a candidate Lyapunov function be given by $V(y) = y^T P y$, where $P \in \mathbf{R^{2\times 2}}$, $P^T = P$, $P \succ 0$ and P satisfies

$$(A - BK)^T P + P(A - BK) + Q \preceq 0, \tag{48}$$

for some $Q \prec 0$. Then, the time derivative of $V(y)$ along the system dynamics (47) is

$$\begin{aligned} \dot{V} &= \dot{y}^T P y + y^T P \dot{y} \\ &= y^T [(A - BK)^T P + P(A - BK)] y \\ &\qquad - 2y^T PB(W - \tilde{f}_2(x, \dot{\epsilon}_d)) \\ &\leq -y^T Q y - 2y^T PB(W - \tilde{f}_2(x, \dot{\epsilon}_d)). \end{aligned} \tag{49}$$

Let

$$W = \beta(x)\mathrm{sgn}(y^T PB), \tag{50}$$

then

$$-2y^T PB(W - \tilde{f}_2(x, \dot{\epsilon}_d)) \leq 0. \tag{51}$$

From Eqs. (49) and (51), we have

$$\dot{V} \leq -y^T Q y < 0. \tag{52}$$

By combining Eqs. (42), (46) and (50), the control input becomes

$$\delta_f = \frac{1}{b_0(x)}(-f_0(x) - Ky - \beta(x)\mathrm{sgn}(y^T PB)), \tag{53}$$

which, in turn, guarantees $V > 0$ and $\dot{V} < 0$. Based on the robust nonlinear stability theory, we have the following theorem.

Theorem 1 *(53) is an asymptotically stabilizing control law for system (22).*

5.2 Comparison of the robust feedback linearization controller with the sliding model controller

The robust feedback linearization based controller given by Eq. (53) is a robust discontinuous controller with a close resemblance to the sliding mode controller given by Eq. (26). If we let the desired trajectory be $y_{sd} = 0$ (corresponding to the lane following case), and denote the sliding mode controller as δ_{fs} to differentiate from the robust feedback linearization based controller, then,

$$\delta_{fs} = \frac{1}{b_0(x)}(-f_0(x) - \lambda\dot{y}_s - (\beta(x) + k)\text{sgn}(\dot{y}_s + \lambda y_s)). \tag{54}$$

On the other hand, the controller (53) can be rewritten as

$$\begin{aligned}\delta_f &= \frac{1}{b_0(x)}(-f_0(x) - k_2\dot{y}_s - k_1 y_s - \beta(x)\text{sgn}(p_{22}\dot{y}_s + p_{12}y_s)) \\ &= \frac{1}{b_0(x)}\left(-f_0(x) - k_2\dot{y}_s - k_1 y_s - p_{22}\beta(x)\text{sgn}\left(\dot{y}_s + \frac{p_{12}}{p_{22}}y_s\right)\right),\end{aligned} \tag{55}$$

where we expand the matrices K and P in their components as

$$K = \begin{bmatrix} k_1 \\ k_2 \end{bmatrix} \qquad \text{and} \qquad P = \begin{bmatrix} p_{11} & p_{12} \\ p_{21} & p_{22} \end{bmatrix}. \tag{56}$$

In terms of the matrix components, the condition that P is symmetric positive definite is equivalent to

$$\begin{aligned} p_{11} &> 0, \\ p_{22} &> 0, \\ p_{12} &= p_{21}, \\ p_{11}p_{22} - p_{12}p_{21} &> 0. \end{aligned} \tag{57}$$

Comparing Eqs. (54) and (55), we see that $\frac{p_{12}}{p_{22}}$ corresponds to λ which defines the sliding surface in the sliding mode control. In the sliding mode control, λ is chosen in such a way that it defines a stable manifold, i.e, $\lambda > 0$. Interestingly, in the feedback linearization design, p_{12} could be a negative number. This is because of the different stabilizing principles in the two controllers. In SMC, the robust control law for δ_f given by Eq. (54) only guarantees that the first order dynamics of the sliding surface, S, is robustly stable, and on the manifold defined by $S = 0$, the choice of λ ensures the stability. It is a two step stabilization strategy. However, in the robust feedback linearization control, the control law for δ_f given by Eq. (55) guarantees the stability of the second order system dynamics by itself.

In the sliding mode control, the coefficient of the discontinuous term is $\beta(x) + k$, whereas in the proposed control, the coefficient of the discontinuous term is $p_{22}\beta(x)$. Note that the matrix inequality (48) holds even when it is mulitplied by a scalar. Therefore, without loss of generality, we can always assume that $p_{22} = 1$. In sliding mode control, the additional positive parameter k is added in the coefficient of the discontinuous term to ensure the finite time convergence of the sliding variable S to the sliding surface defined by $S = 0$, and therefore it is not desirable to select k too small. Once the sliding surface is reached in a finite time, the system states go to the equilibrium asymptotically while staying on the manifold. In feedback linearization, all the states goes to the equilibrium point asymptotically in the state space. It is not difficult to see that the sliding mode controller inevitably results in a higher gain controller and degrades riding comfort. The situation remains the same when saturation functions replace the sign functions to reduce chattering in both feedback linearization controller and sliding mode controller.

For fairness of comparison, we modify the SMC as

$$\delta_f = \frac{1}{b_0(x)}(-f_0(x) - \lambda\dot{y}_s - k(\dot{y}_s + \lambda y_s) - \beta(x)\text{sgn}(\dot{y}_s + \lambda y_s)). \tag{58}$$

Comparing the modified sliding mode controller (58) and the feedback linearization controller (55) and assuming that there is no model uncertainties, i.e. $\beta(x) = 0$,

we note that both Eq. (55) and (58) stabilize the linear system (44). In the case of modified sliding mode control, the characteristic equation of the closed loop system is

$$s^2 + (\lambda + k)s + \lambda k = 0, \tag{59}$$

and in the case of feedback linearization based control, it is

$$s^2 + k_2 s + k_1 = 0. \tag{60}$$

As we can see, in the modified sliding mode control, the dynamics of the sliding surface/manifold and that of the nominal system is coupled, whereas, in the robust feedback linearization control, the dynamics of the "sliding surface" and that of the nominal plant are decoupled. If we can find a positive definite matrix P satisfying the linear matrix inequality(48) with $p_{22} < 1$, we are equivalently "minimizing" the bound of the model uncertainties. It is obvious that we always can find such a P, by simultaneously scaling P and Q in (48).

Both in the robust feedback linearization control and SMC, we assume that the zero dynamics of the system is exponentially stable and the designed controllers robustly stabilize the dynamics in the r dimensional controllable subspace, where, r is the relative degree of the system dynamics. In the SMC, the r dimensional controllable subspace is described as a set of $r-1$ dimensional stable submanifolds, i.e. one dimensional vector space, and the stability is achieved in two stages: first the one dimensional submanifold space is forced to converge to 0, i.e. the stable sliding surface, by the robust term in the sliding mode control law and then, from the stability of the sliding surface, the system states converge to zero while staying within the sliding surface. In the robust feedback linearization controller, the controller forces the states in the r dimensional controllable subspace go to zero. Hence, there is no stability requirement for the submanifold, $y^T PB = 0$.

Another thing that we would like to point out is that, we can optimally select the control parameters in the robust feedback linearization control method based

on some performance criteria, possibly using Linear Matrix Inequality (LMI) based computational tools such as Semi-Definite Programming (SDP).

5.3 Simulation results

In the design of robust controllers, we assumed that the model uncertainties are bounded by a know function (Assumption 1). In practice it is very hard to evaluate the uncertainty bounds. In our simulations, the tire cornering stiffness is perturbed by 30% to introduce more uncertainties in addition to the unmodeled nonlinear dynamical uncertainties. We assume that the uncertainty bound for $\tilde{f}_2(q, \dot{q})$ is time and state invariant, i.e. $\beta(x) = \beta$. To estimate the uncertainty bound, the control parameter k is set to zero in the sliding mode controller (54), and we repeatedly run simulations by increasing β by a small amount ($\Delta\beta$) each time. We expect that when β changes from some value smaller than the true bound, say β^*, to some value larger than the true value, the system will change from an unstable system to a stable one. Since, β is increased by a finite amount in each simulation, the uncertainty bound is determined to be the value at which stability is attained for the first time. This procedure should be repeated for each selected simulation scenarios.

The simulation scenario for a tractor-semitrailer travelling at a velocity of $60mph$ is as follows. Initially the vehicle travels on a straight section for 0.5 second; at $t = 0.5sec$, it enters a curved section with a radius of $600m$; and at $t = 3sec$, it leaves the curved section and continues to run on a straight section. By the method mentioned above, we conclude that the uncertainty bound β is 0.30. In Fig. 8, the four dotted lines, from large to small excursions, are the simulation results of the SMC with $k = 0.01$ and $\beta = 0.30,\ 0.33,\ 0.35$ and 0.37, respectively, similarly the four solid lines are the simulation results of the robust feedback linearization controller with $K = [2,\ 1]^T$, $Q = [1\ 0;\ 0\ 1]$ and $\beta = 0.30,\ 0.33,\ 0.35$ and 0.37, respectively. The upper left plot is the designed control input, the lower left plot is the lateral error at the center of gravity of the tractor, the upper right plot is the relative yaw error of

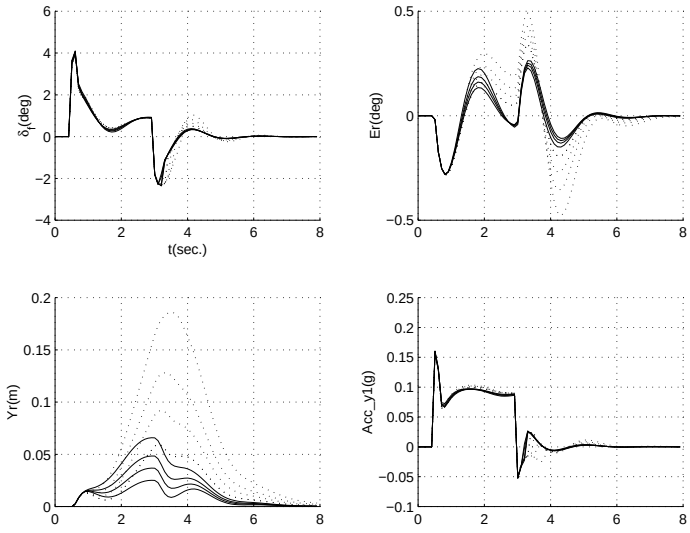

Figure 8: Simulation Results–Solid:Feedback Linearization Control; Dashed:Sliding Model Control

the tractor and the lower right plot is the lateral acceleration of the tractor.

From the plot of the lateral error and the relative yaw error of the tractor, we see that SMC is very sensitive to the knowledge of the uncertainty bound, and once the bound is known, any positive number k stabilizes the system. In the robust feedback linearization control, due to the $-y^T Qy$ term in $\dot{V}$, even a use of smaller estimate of the uncertainty bound can stabilize the system. SMC is a robust stabilizing controller and it is very hard to incorporate performance criteria in controller design, while in the case of the robust feedback linearization control, it is easy to incorporates performance criteria in the controller design with different selections of K and Q and there is possibility of optimally selecting the control parameters based on performance criteria using the semidefinite programming.

6 Nonlinear Robust Loop-Shaping Controller Considering Steering Subsystem Dynamics

In the above mentioned controllers, the sliding mode controller, adaptive robust controller and the robust feedback linearization controller, the control input is the front wheel steering angle designed based on the vehicle body dynamics. In practice, the control signals are feeded into the steering actuator mounted on the steering column, and the steering actuator moves the front steering wheel through the torsion bar on the steering column, the hydraulic power assist unit and the front wheel assembly. The dynamics of the steering subsystem is very complicated [1]. Therefore, the dynamics of the vehicle lateral control system can be thought of a cascaded connection of the steering subsystem dynamics and the vehicle body dynamics. We adopt a nested control structure, i.e., we first design a controller (called an inner-loop controller) for the steering subsystem so that the local closed-loop steering subsystem has a very good tracking performance, and then design a controller (called an outer-loop controller) for the vehicle body dynamics by either ignoring the closed-loop steering subsystem dynamics or by approximating it by a simple lower order dynamics. The previously designed controllers belong to the former case. In this section, we model the dynamics of the closed-loop steering subsystem as a first order linear dynamical system with model uncertainty. To prevent the actuator saturation and reduce chattering while explicitly taking into account the vehicle model uncertainty and actuator model uncertainty in the controller design, we propose to extend the vehicle lateral control system dynamics with a low-pass filter (in this study, we use first order filter) at the input side of the steering actuator. The added pre-filter is also to filter sensor noise. The input to the augmented system is the input to the pre-filter and because the model uncertainties are not in the same channel as control input, the robust slid-

[1]The steering subsystem of the tractor-semitrailer type of heavy vehicle systems was studied under MOU 313 and reported in California PATH Working Paper UCB-ITS-PWP-2000-1

ing mode control technique can not be directly applied. We apply the constructive backstepping method [18] together with the smooth robust control technique to the extended system. The actual control input to the steering actuator is the output of the pre-filter.

6.1 Model description

Steering subsystem: The steering system is a critical component of the vehicle lateral control system. From the viewpoint of vehicle lateral control, the front wheel steering angle is often regarded as the control input. The actual control input, however, is the command signal to the actuator which is set by the lateral controller. Thus, to improve the system performance, the dynamics of the steering subsystem must be considered along with the vehicle lateral body dynamics in the design of vehicle lateral controllers.

As mentioned already, the California PATH uses a Freightliner class 8 truck as an experimental test vehicle. The existing steering system on the Freightliner truck has been retrofitted with an electric steering actuator mounted directly on the steering column of the existing steering system. Then, an inner-loop controller is designed for the steering subsystem to let the steering wheel track the desired trajectory set by the vehicle lateral controller. With the inner-loop controller, the local closed-loop steering system is modeled as a first order linear system with model uncertainty as

$$\dot{\delta}_f = \frac{1}{\tau_a}(\delta_a - \delta_f) + \Delta(x, \delta_f), \tag{61}$$

where δ_a is the input to the steering actuator and τ_a is the time constant.

Augmented lateral control model: The steering system has a physical limit in the steering angle and the steering actuator has a limit in the slew rate. To prevent the actuator saturation and reduce chattering while explicitly taking into account the vehicle model uncertainties and actuator model uncertainties in the controller design,

the vehicle lateral dynamics is augmented by a first order pre-filter,

$$\delta_a(S) = \frac{1}{\tau_1 S + 1} u(S), \tag{62}$$

at the input side of the steering actuator, where u is the control input we are going to design.

From Eqs. (22), (61) and (62), the lateral control model of the tractor-semitrailer system with steering system dynamics and pre-filter can be written as

$$\begin{aligned} \dot{x} &= b_{x0}(x)\delta_f + f_{x0}(x) + \tilde{f}_{x2}(x), \\ \ddot{y}_s &= b_0(x)\delta_f + f_0(x) + \tilde{f}_2(x,t), \\ \dot{\delta}_f &= \frac{1}{\tau_a}(\delta_a - \delta_f) + \Delta(x, \delta_f), \\ \dot{\delta}_a &= \frac{1}{\tau_1}(u - \delta_a). \end{aligned} \tag{63}$$

In the above system, x is the state variable, $b_{x0}(x)$, $f_{x0}(x)$, $b_0(x)$ and $f_0(x)$ are known functions, and $\tilde{f}_{x2}(x)$, $\tilde{f}_2(x,t)$ and $\Delta(x, \delta_f)$ are functions used to represent model uncertainties including both unmodeled nonlinear dynamical uncertainties and parametric uncertainties. Considering the physical properties of the system, the following reasonable assumptions are made.

Assumption 5 *The unknown nonlinear functions are bounded above by known functions, i.e.,*

$$\begin{aligned} \|\tilde{f}_2\| &\leq \beta(x), \\ \|\tilde{f}_{x2}\| &\leq \beta_x(x), \\ \|\Delta\| &\leq \beta_1(x, \delta_f), \end{aligned} \tag{64}$$

where $\beta(x) \in C^3(x)$, $\beta_x(x) \in C^3(x)$ and $\beta_1(x, \delta_f) \in C^3(x, \delta_f)$ are known functions.

Assumption 6 *$b_0(x)$ and $b_{x0}(x)$ are positive functions.*

Note that the first assumption is about the extent of model uncertainties. The second assumption is to ensure that the input gain for the first two equations of (63)

are nonzero all the time. The objective is to design a control law for u such that the output y_s tracks the desired trajectory $y_{sd}(t)$ as close as possible. Since the model uncertainties, $\tilde{f}_{x2}, \tilde{f}_2$ and Δ, do not satisfy the model matching condition, we use the backstepping method.

6.2 Controller design

The lateral position at the virtual sensor location, y_s, has relative degree of two with respect to the front wheel steering input, δ_f. Let the sliding variable[2] be defined as

$$S = \dot{e} + \lambda e, \tag{65}$$

where $e = y_s - y_{sd}$ is the output tracking error and λ is a positive constant design parameter. To avoid large input when the initial tracking error $e(0)$ is large, we modify the sliding variable as

$$\bar{S} = S - S(0)\exp(-\lambda_1 t), \tag{66}$$

where λ_1 is a positive number. Define

$$\tilde{\delta}_f(x, \delta_f, t) = \alpha_1(x, t) - \delta_f, \tag{67}$$

where $\alpha_1(x, t)$ is the desired front wheel steering angle which will be synthesized later. From Eq. (63),

$$\begin{aligned} \dot{\bar{S}} &= b_0(x)\delta_f + f_0(x) + \tilde{f}_2(x, t) - \ddot{y}_{sd} + \lambda\dot{e} + \lambda_1 S(0)\exp(-\lambda_1 t) \\ &= b_0(x)\alpha_1(x, t) + f_0(x) - \ddot{y}_{sd} + \lambda\dot{e} + \lambda_1 S(0)\exp(-\lambda_1 t) \\ &\quad + \tilde{f}_2(x, t) - b_0(x)\tilde{\delta}_f(x, \delta_f, t). \end{aligned} \tag{68}$$

Choose $\alpha_1(x, t)$ as

$$\alpha_1(x, t) = -\frac{1}{b_0(x)}\left(f_0(x) - \ddot{y}_{sd} + \lambda\dot{e} + \lambda_1 S(0)\exp(-\lambda_1 t) + \left(c_1 + \frac{\beta^2(x)}{4\epsilon_1}\right)\bar{S}\right), \tag{69}$$

[2] S is called the sliding variable although the exact sliding is not attempted here in order to avoid chattering. For example, Eq.(69) involves a term proportional to S instead of a sign function of S

where c_1 and ϵ_1 are positive constants. Define the candidate Lyapunov function be

$$V_1 = \frac{1}{2}\bar{S}^2. \tag{70}$$

Then, from Eqs. (67), (68), (69) and (70), we have

$$\begin{aligned} \dot{V}_1 &= \bar{S}\dot{\bar{S}} \\ &\leq -c_1\bar{S}^2 + \tilde{f}_2\bar{S} - \frac{\beta^2}{4\epsilon_1}\bar{S}^2 - b_0(x)\bar{S}\tilde{\delta}_f \\ &\leq -c_1\bar{S}^2 + \epsilon_1 - b_0(x)\bar{S}\tilde{\delta}_f, \end{aligned} \tag{71}$$

which means that if $\tilde{\delta}_f = 0$, i.e., if the output of the steering system tracks the desired front wheel steering angle α_1 exactly, then the sliding variable asymptotically converges to a ball whose size is defined by ϵ_1. From Eq. (69),

$$\begin{aligned} \dot{\alpha}_1(x,t) &= \frac{\partial \alpha_1}{\partial x}\dot{x} + \frac{\partial \alpha_1}{\partial t} \\ &= \frac{\partial \alpha_1}{\partial x}(b_{x0}(x)\delta_f + f_{x0}(x) + \tilde{f}_{x2}(x)) + \frac{\partial \alpha_1}{\partial t}. \end{aligned} \tag{72}$$

Define $\hat{\dot{\alpha}}_1$ and $\tilde{\dot{\alpha}}_1$ as

$$\begin{aligned} \hat{\dot{\alpha}}_1(x,t) &= \frac{\partial \alpha_1}{\partial x}\left(b_{x0}(x)\delta_f + f_{x0}(x)\right) + \frac{\partial \alpha_1}{\partial t}, \\ \tilde{\dot{\alpha}}_1(x,t) &= \frac{\partial \alpha_1}{\partial x}\tilde{f}_{x2}(x), \end{aligned} \tag{73}$$

then

$$\dot{\alpha}_1(x,t) = \hat{\dot{\alpha}}(x,t) + \tilde{\dot{\alpha}}_1(x,t). \tag{74}$$

Modify the Lyapunov function candidate V_1 to

$$V_2 = V_1 + \frac{1}{2\Gamma_1}\tilde{\delta}_f^2, \tag{75}$$

where Γ_1 is a positive control parameter. Then,

$$\begin{aligned}
\dot{V}_2 &= \dot{V}_1 + \frac{1}{\Gamma_1}\tilde{\delta}_f\dot{\tilde{\delta}}_f \\
&\leq -c_1\bar{S}^2 + \epsilon_1 - b_0(x)\bar{S}\tilde{\delta}_f \\
&\quad + \frac{1}{\Gamma_1}\tilde{\delta}_f\left(\hat{\dot{\alpha}}_1(x,t) + \tilde{\dot{\alpha}}_1(x,t) - \frac{1}{\tau_a}\left(\delta_a - \delta_f\right) - \Delta(x,\delta_f)\right) \\
&\leq -c_1\bar{S}^2 + \epsilon_1 \\
&\quad + \frac{1}{\Gamma_1}\tilde{\delta}_f\left(-\Gamma_1 b_0(x)\bar{S} + \hat{\dot{\alpha}}_1(x,t) + \tilde{\dot{\alpha}}_1(x,t) - \frac{1}{\tau_a}\left(\delta_a - \delta_f\right) - \Delta(x,\delta_f)\right).
\end{aligned} \tag{76}$$

Let the desired input to the steering actuator be

$$\alpha_2(x,\delta_f,t) = \delta_f + \tau_a\left(-\Gamma_1 b_0(x)\bar{S} + \hat{\dot{\alpha}}_1(x,t) + \Gamma_1\left(c_2 + \frac{\beta_2^2(x,\delta_f,t)}{4\epsilon_2}\right)\tilde{\delta}_f\right), \tag{77}$$

where c_2 and ϵ_2 are positive control parameters and $\beta_2(x,\delta_f,t)$ is a know function satisfying

$$\left\|\frac{1}{\Gamma_1}(\tilde{\dot{\alpha}}_1(x,t) - \Delta(x,\delta_f))\right\| \leq \beta_2(x,\delta_f,t). \tag{78}$$

Define

$$\tilde{\delta}_a(x,\delta_f,\delta_a,t) = \alpha_2(x,\delta_f,t) - \delta_a, \tag{79}$$

then, from Eqs. (76), (77), (78) and (79),

$$\begin{aligned}
\dot{V}_2 &\leq -c_1\bar{S}^2 + \epsilon_1 - c_2\tilde{\delta_f}^2 + \frac{1}{\Gamma_1}\left(\tilde{\dot{\alpha}}_1 - \Delta\right)\tilde{\delta}_f - \frac{\beta_2^2}{4\epsilon_2}\tilde{\delta}_f^2 + \frac{1}{\Gamma_1}\tilde{\delta}_f\frac{\tilde{\delta}_a}{\tau_a} \\
&\leq -c_1\bar{S}^2 + \epsilon_1 - c_2\tilde{\delta_f}^2 + \epsilon_2 + \frac{1}{\Gamma_1\tau_a}\tilde{\delta}_f\tilde{\delta}_a.
\end{aligned} \tag{80}$$

From Eq. (77),

$$\begin{aligned}
\dot{\alpha}_2(x,\delta_f,t) &= \frac{\partial\alpha_2}{\partial x}\dot{x} + \frac{\partial\alpha_2}{\partial\delta_f}\dot{\delta}_f + \frac{\partial\alpha_2}{\partial t} \\
&= \hat{\dot{\alpha}}_2(x,\delta_f,t) + \tilde{\dot{\alpha}}_2(x,\delta_f,t),
\end{aligned} \tag{81}$$

where

$$\begin{aligned}
\hat{\dot{\alpha}}_2(x,\delta_f,t) &= \frac{\partial\alpha_2}{\partial x}(b_{x0}(x)\delta_f + f_{x0}(x)) + \frac{\partial\alpha_2}{\partial\delta_f}\frac{\delta_a - \delta_f}{\tau_a} + \frac{\partial\alpha_2}{\partial t}, \\
\tilde{\dot{\alpha}}_2(x,\delta_f,t) &= \frac{\partial\alpha_2}{\partial x}\tilde{f}_{x2}(x) + \frac{\partial\alpha_2}{\partial\delta_f}\Delta(x,\delta_f).
\end{aligned} \tag{82}$$

Now, we design the control input u such that the input to the steering actuator follows α_2. Define the candidate Lyapunov function as

$$V = V_2 + \frac{1}{2\Gamma_2}\tilde{\delta}_a^2, \tag{83}$$

where Γ_2 is a positive control parameter. Then,

$$\begin{aligned}
\dot{V} &= \dot{V}_2 + \frac{1}{\Gamma_2}\tilde{\delta}_a\dot{\tilde{\delta}}_a \\
&= -c_1\bar{S}^2 + \epsilon_1 - c_2\tilde{\delta}^2 + \epsilon_2 \\
&\quad + \frac{1}{\Gamma_1\tau_a}\tilde{\delta}_f\tilde{\delta}_a + \frac{1}{\Gamma_2}\tilde{\delta}_a(\dot{\hat{\alpha}}_2(x,\delta_f,t) + \dot{\tilde{\alpha}}_2(x,\delta_f,t) - \frac{1}{\tau_1}(u-\delta_a)) \\
&= -c_1\bar{S}^2 + \epsilon_1 - c_2\tilde{\delta}^2 + \epsilon_2 \\
&\quad + \frac{1}{\Gamma_2}\tilde{\delta}_a\left(\frac{\Gamma_2}{\Gamma_1\tau_a}\tilde{\delta}_f + \dot{\hat{\alpha}}_2(x,\delta_f,t) + \dot{\tilde{\alpha}}_2(x,\delta_f,t) - \frac{1}{\tau_1}(u-\delta_a)\right).
\end{aligned} \tag{84}$$

Choose u as

$$u(x,\delta_f,\delta_a,t) = \delta_a + \tau_1\left(\frac{\Gamma_2}{\Gamma_1\tau_a}\tilde{\delta}_f + \hat{\dot{\alpha}}_2(x,\delta_f,t) + \Gamma_2(c_3 + \frac{\beta_3^2(x,\delta_f,t)}{4\epsilon_3})\tilde{\delta}_a\right), \tag{85}$$

where c_3 and ϵ_3 are positive constants and $\beta_3(x,\delta_f,t)$ is a known function satisfying

$$\|\frac{1}{\Gamma_2}\dot{\tilde{\alpha}}_2(x,\delta_f,t)\| \le \beta_3(x,\delta_f,t). \tag{86}$$

From Eqs. (84), (85) and (86), we finally have

$$\dot{V} = -c_1\bar{S}^2 + \epsilon_1 - c_2\tilde{\delta}_f^2 + \epsilon_2 - c_3\tilde{\delta}_a^2 + \epsilon_3. \tag{87}$$

The following theorem can readily be proved using the above arguments.

Theorem 2 *If the internal dynamics of the system given by Eq. (63) is stable, then the robust backstepping control law (85) guarantees that the resulting closed-loop system is globally stable and the output tracking error e converges to a ball, whose size depends on ϵ_1, ϵ_2 and ϵ_3.*

6.3 Simulation results

We have simulated two controllers for two different plants under different road conditions and results are shown in Figs. 9, 10 and 11. Controller-A is a controller designed without explicitly taking into account the steering actuator dynamics, i.e., α_1 given by Eq. (69) is considered to be the steering input, δ_f. Controller-B is the controller proposed in this section which includes the steering actuator dynamics in the system model and dynamically extends it with a first order filter. The two plants we considered are: Plant-A, without actuator dynamics, and Plant-B, with first order actuator dynamics. Figures 9 and 10 show the simulation results when the vehicle model has only unmodeled nonlinear dynamical uncertainties and the system parameters are all known. Figure 11 shows the simulation results of the vehicle model with 30% of parametric uncertainty in the tire cornering stiffness, $C_{\alpha f}$, $C_{\alpha r}$ and $C_{\alpha t}$, in addition to the unmodeled nonlinear dynamical uncertatinties. Each figure shows, from the left-upper plot to the right-bottom plot, the front wheel steering angle, tractor yaw error relative to the road, lateral error at the c.g. of the tractor, lateral acceleration of c.g. of the tractor, articulation angle and tractor yaw rate.

As we can see from the simulation results, when Controller-A is applied to Plant-B (actual system) it has severe oscillations (dashed lines in Fig. 9, $c_1 = 4.0$); as we decrease the controller gain, c_1, the oscillation mode becomes less severe, but, the magnitude of the front wheel steering angle becomes larger (dashdotted ($c_1 = 8.0$) and dashed ($c_1 = 20.0$) lines in Fig. 10). On the other hand, Controller-B (solid line in Fig. 10) provides smoother response and smaller front wheel steering angle. When there are parametric uncertainties in the tire cornering stiffness (Fig. 11), similar phenomena show up as in the case when there is no parametric uncertainties. In Fig. 11, dotted lines represent the simulation results of Controller-B; solid, dashed and dashdotted lines represent the simulation results of Controller-A with the feedback gain, c_1, in the increasing order. The larger the size of the model uncertainties, the higher the resulting control gain of the traditional robust controllers such as SMC [26]. Ac-

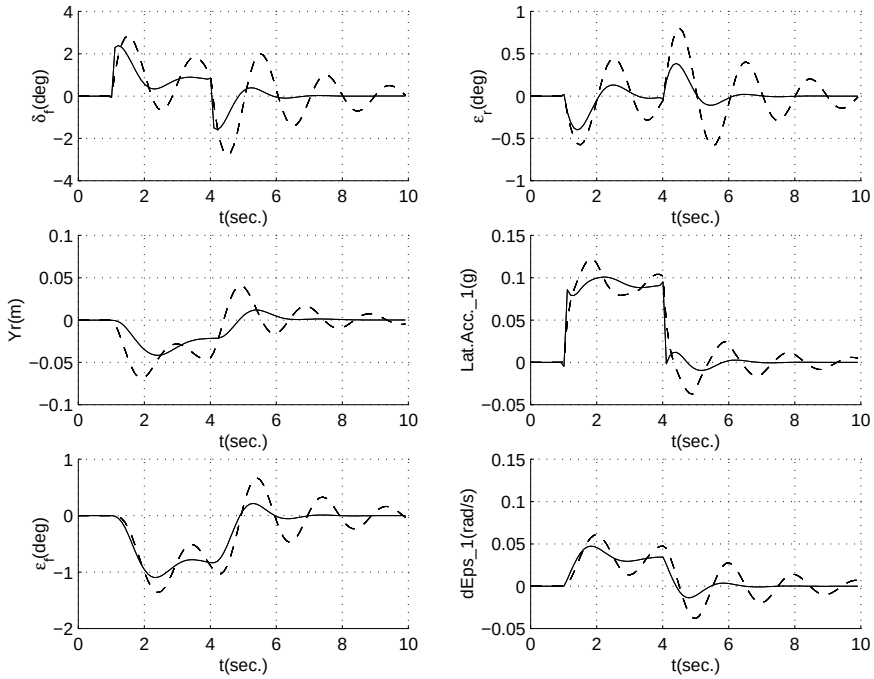

Figure 9: Simulation Results-1 of the Nonlinear Robust Loop-Shaping Controller

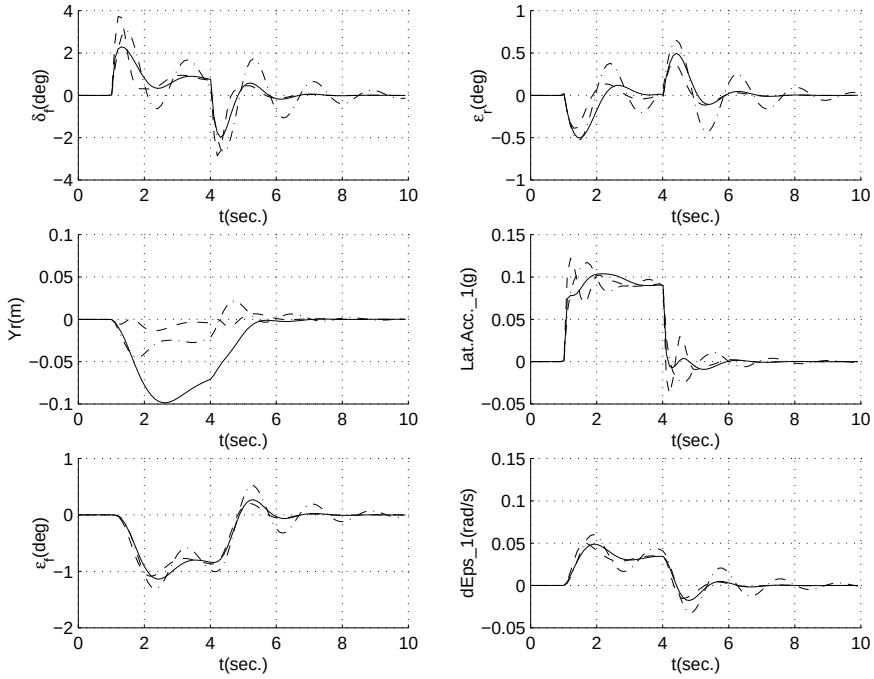

Figure 10: Simulation Results-2 of the Nonlinear Robust Loop-Shaping Controller

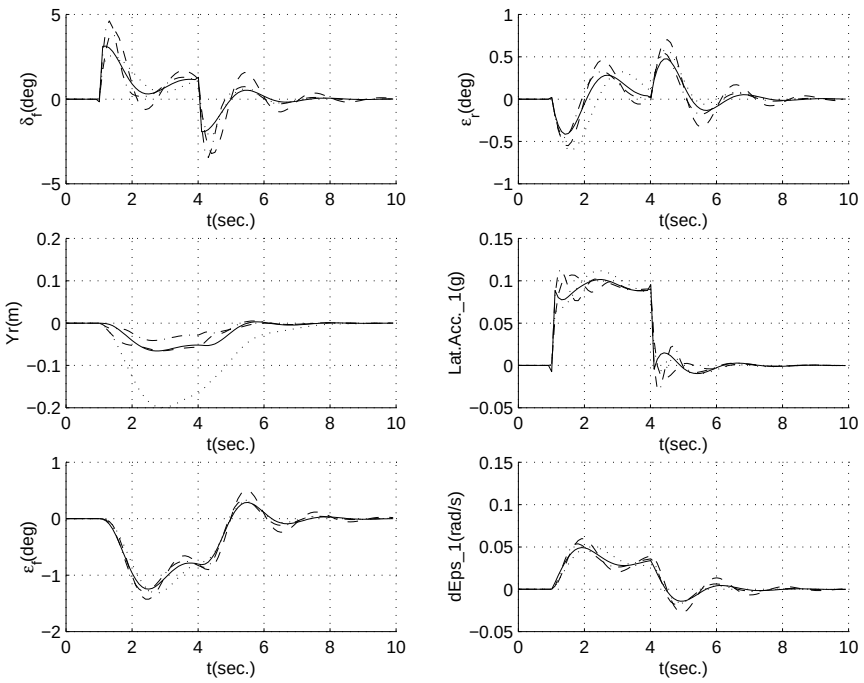

Figure 11: Simulation Results-3 of the Nonlinear Robust Loop-Shaping Controller

cordingly, in the case of larger model uncertainties, the effective control gain reduction for assurance of stability and riding comfort (smootheness) is more imperative. Note that Controller-B has a larger tracking error than Controller-A in each simulation scenarios, though they are all within the acceptable limit, $0.2m$.

7 Linear Robust Feedback Controller with Feedforward Compensation

Nonlinear controllers are usually designed based on a more detailed nonlinear model of a system and assumes more knowledge of the system to be controlled. Therefore, in theory, they should provide better performances than linear controllers designed based on an approximated, linearized model of the actual system. However, nonlinear controllers are more costly in terms of implementation and sometimes it is impractical to implement them at all. On the other hand, there are rich design methodologies

and software tools are available for the design of linear controllers.

In this section, we investigate a possible mid-ground for ease of implementation and high performance by exploring and taking advantages of the inherent structure of the vehicle lateral control system with an example of a tractor-semitrailer heavy vehicle system with an example of a tractor-semitrailer combination.

7.1 Linear model of a tractor-semitrailer vehicle system

From Eq. (3), we get

$$\begin{aligned} \varepsilon_1 &= \varepsilon_r + \varepsilon_d, \\ \dot{\varepsilon}_1 &= \dot{\varepsilon}_r + \dot{\varepsilon}_d, \\ \ddot{\varepsilon}_1 &= \ddot{\varepsilon}_r + \ddot{\varepsilon}_d, \end{aligned} \tag{88}$$

and from Eq. (10), we have

$$V_y = \dot{y}_r - \varepsilon_r V_x. \tag{89}$$

By substituting Eqs. (88) and (89) in Eq. (1) and linearizing it, we get the linear control model of a tractor-semitrailer vehicle system in the road coordinate system as

$$\begin{aligned} &M_r \ddot{q}_r + D_r \dot{q}_r + K_r q_r = F_r \delta_f + E_1 \dot{\varepsilon}_d(t) + E_2 \ddot{\varepsilon}_d(t), \\ &y_s = \begin{pmatrix} 1 & d_s & 0 \end{pmatrix}^T q_r, \end{aligned} \tag{90}$$

where

$$q_r = \begin{pmatrix} y_s, \varepsilon_r, \varepsilon_f \end{pmatrix}^T. \tag{91}$$

The matrices, M_r, D_r, K_r, F_r, E_1 and E_2, are as given in Appendix B. In the above generalized coordinates, y_r is the lateral displacement of the tractor's center of gravity, ε_r is the tractor's yaw error in the road coordinate system and ε_f is the articulation angle. The system input is tractor's front wheel steering angle δ_f and the system output y_s is the lateral tracking error of the virtual sensor located at the look-ahead distance of d_s. In Eq. (90), $\dot{\varepsilon}_d$ and $\ddot{\varepsilon}_d$ are desired tractor's yaw rate and rate of change

of the desired yaw rate, respectively, and they are treated as disturbances to the system. $\dot{\varepsilon}_d$ is related to the vehicle speed V_x and road curvature ρ by Eq. 2. Defining a 6×1 state vector as

$$x_r = \begin{pmatrix} q_r \\ \dot{q}_r \end{pmatrix}. \tag{92}$$

Then, the linear state-space model of the vehicle lateral control system is obtained as

$$\begin{aligned} \dot{x}_r = & \begin{pmatrix} 0 & I \\ -M_r^{-1}K_r & -M_r^{-1}D_r \end{pmatrix} x_r + \begin{pmatrix} 0 \\ M_r^{-1}F_r \end{pmatrix} \delta_f \\ & + \begin{pmatrix} 0 \\ M_r^{-1}E_1 \end{pmatrix} \dot{\varepsilon}_d + \begin{pmatrix} 0 \\ M_r^{-1}E_2 \end{pmatrix} \ddot{\varepsilon}_d. \end{aligned} \tag{93}$$

It is noted that the system matrices in Eqs. (90) and (93) depend on the vehicle speed, tire cornering stiffness and load configuration on the trailer. Details of this aspect are documented in [29].

Notice that the desired yaw rate, $\dot{\varepsilon}_d$, appears in the linearized model. In designing linear controllers, the $\dot{\varepsilon}_d$-related terms are treated as disturbances coming from the road, and linear controllers are designed so that they not only reject the road disturbances but also other disturbances such as wind gust. In the presence of such disturbances, the steady-state tracking error is directly affected by the P gain of the controller. The larger the P gain, the smaller the steady-state tracking error. On the other hand, a lager P gain may excite unmodeled dynamics and may induce oscillations.

7.2 Controller design

By examining the sources of the road disturbances and the ways they enter the model equations, we find the following analogy between the lateral dynamics of a vehicle system and the dynamics of a mechanical system with Coulomb friction.

When a vehicle is riding on a straight road section, $\dot{\varepsilon}_d$ is zero, and therefore there is no road disturbance. When the vehicle is negotiating a curve and turning left,

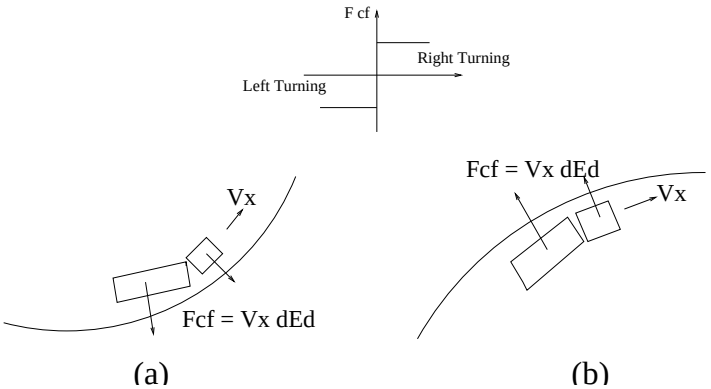

Figure 12: Centrifugal Forces of a Vehicle Negotiating a Curve

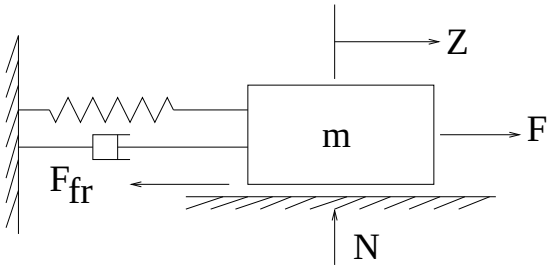

Figure 13: Coulomb Friction in a Mass-Spring-Damper System

there are centrifugal forces acting at the centers of gravity of the tractor and of the semitrailer. These centrifugal forces point right and their magnitude is proportional to $V_x\dot{\varepsilon}_1$ as shown in Fig. 12(a). When the vehicle is turning right, the centrifugal forces are proportional to $V_x\dot{\varepsilon}_1$ and they point left as shown in Fig. 12(b). In other words, the centrifugal forces are proportional to $-V_x\dot{\varepsilon}_1$ and are discontinuous.

Recall that, for mechanical systems with Coulomb friction (cf. Fig. 13), the Coulomb friction forces are proportional to $-\dot{x}$ and discontinuous. That is, the centrifugal forces of a vehicle negotiating a curve are analogous to the Coulomb friction forces.

For a mechanical system with Coulomb friction forces, if they can be obtained or estimated, adding a feedforward term to compensate for the disturbances (the friction forces) is a practical and efficient approach. Motivated by this, we design a feedforward controller to compensate for the road disturbances in addition to a linear

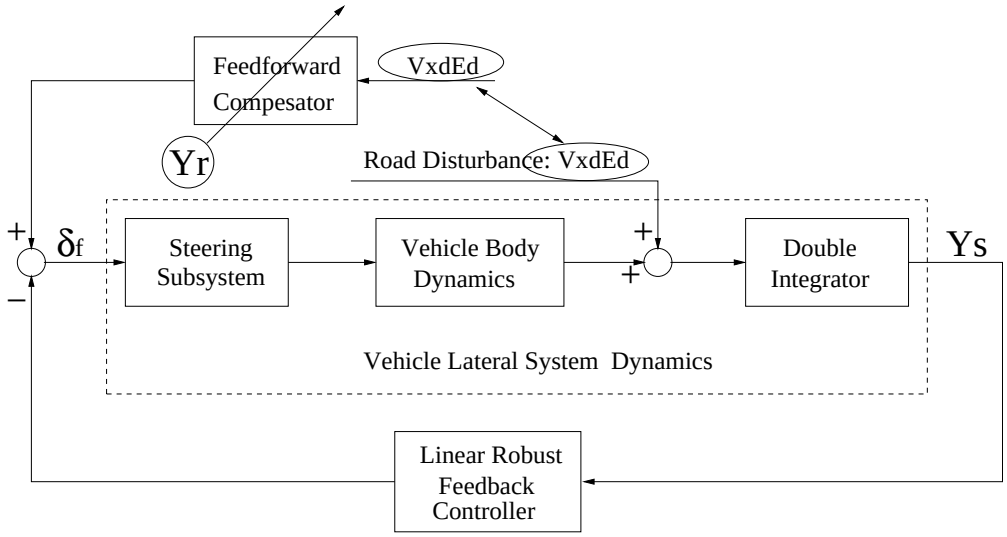

Figure 14: Diagram of Feedforward Compensation for the Lateral Control of a Heavy Vehicle System

robust feedback controller as shown in Fig. 14. We take the input to the feedforward compensator as $V_x\dot{\varepsilon}_d$. As such, the feedforward compensator has a built-in switch to turn on and off the compensator based on needs. That is, when the vehicle is negotiating a curve, $\dot{\varepsilon}_d$ is nonzero and therefore the feedforward compensator is on, and when the vehicle is travelling on a straight section, $\dot{\varepsilon}_d$ is zero and therefore the switch is off.

A possible candidate for the feedforward compensator is the inverse dynamics of the system, from the road disturbances $V_x\dot{\varepsilon}_d$ to the output y_s. But, as we have learned, the vehicle dynamics has model uncertainties and it may not exactly compensate for the disturbances as we expect. We propose to use a constant gain feedforward compensator with the constant equal to the inverse of the linear gain of the disturbance dynamics. This gain is a function of vehicle inertia and dimensional parameters as well as tire cornering stiffness. To account for the parametric uncertainties in the constant feedforward compensator, we introduce an adaptation to the constant gain based on the lateral tracking error at the c.g. of the tractor.

7.3 Simulation results

The simulation scenario is as given in subsection 3.3. We simulated three controllers: a) without feedforward compensation, b) with a constant gain feedforward compensation, and c) with adaptive feedforward compensation. The feedback controller used in simulations of the three controllers is a linear robust loop-shaping controller. From Fig. 15, we see that the feedforward compensator effectively reduces the lateral tracking error and provides a smoother control input. The adaptive feedforward compensator reduces the tracking error even further.

7.4 Comparison with nonlinear robust controllers

Recall that the nonlinear robust controllers, such as a sliding mode controller, involve a feedback linearization term. From Eq. (16), the output dynamics of the vehicle lateral control system can be reformatted as

$$\begin{aligned} \ddot{y}_s &= \dot{V}_y + d_s\ddot{\varepsilon}_1 + V_x\dot{\varepsilon}_r \\ &= (\dot{V}_y + V_x\dot{\varepsilon}_1 + d_s\ddot{\varepsilon}_1) - V_x\dot{\varepsilon}_d \\ &= f(x) + b(x)\delta_f - V_x\dot{\varepsilon}_d. \end{aligned} \tag{94}$$

Then, the nonlinear controllers have the form of

$$\begin{aligned} \delta_f &= -\frac{1}{b(x)}(f(x) - V_x\dot{\varepsilon}_d + \cdots) + \cdots \\ &= \frac{1}{b(x)}(V_x\dot{\varepsilon}_d) - \frac{1}{b(x)}(f(x) + \cdots) + \cdots . \end{aligned} \tag{95}$$

Equation (95) suggests that the nonlinear controllers inherently have a feedforward compensation which corresponds to the fixed gain feedforward control. For comparison, Fig. 16 shows the simulations results of a sliding mode controller and the above mentioned three linear robust controllers. As we can see from the figure, the sliding mode controller offers the best tracking performance as expected. However, as we will see in section 8, the implementation of nonlinear controllers is not trivial and much harder than that of linear controllers. Therefore, linear robust controllers with

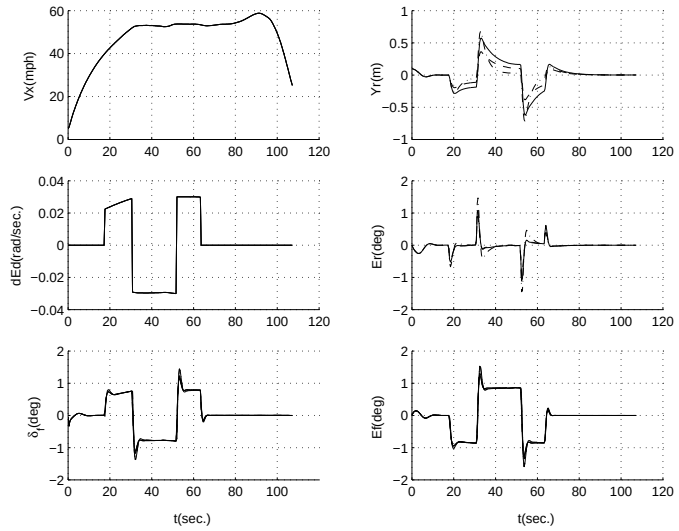

Figure 15: Simulation Results of Linear Robust Controllers with Feedforward Compensation: Solid: Without Feedforward Compensation, Dashed: With Constant Gain Feedforward Compensation, Dash-Dot: With Adaptive Feedforward Compensation

feedforward compensators are a mid-point between liner feedback controllers and nonlinear controllers from the view point of ease of implementation and control system performance.

8 Experiments

This section presents various experimental aspects of the lateral control of heavy vehicles for automated driving such as the hardware and software setup of the experimental vehicle, the open-loop tests and system parameter estimation, experimental issues, and closed-loop tests for different controllers. Three controllers, a sliding mode controller, a linear feedback controller with a feedforward compensation and a linear feedback controller, are compared by analysis and by experiments. These three controllers are closely related to one another by means of the constituting terms of the controllers. The experiments were conducted on the test vehicle, a tractor-semitrailer combination, at a 2000m long test track at Crows Landing.

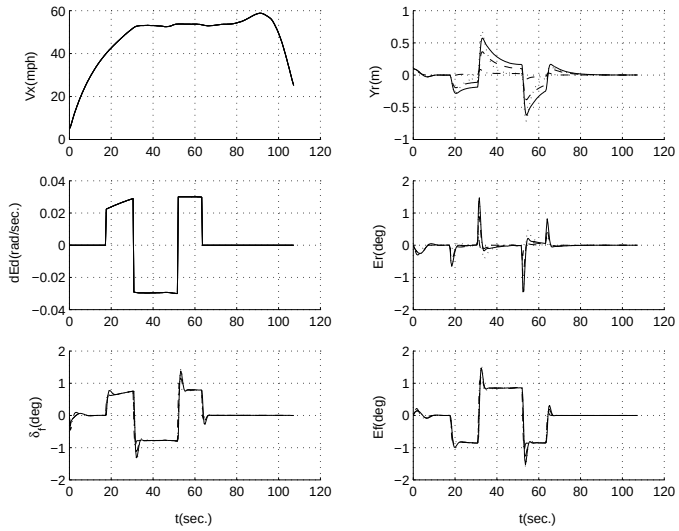

Figure 16: Comparison of Nonlinear Controllers with Linear Robust Controllers with Feedforward Compensation: Solid: Without Feedforward Compensation, Dashed: With Constant Gain Feedforward Compensation, Dotted: With Adaptive Feedforward Compensation, Dash-Dot: Sliding Mode Controller

8.1 Structural analysis of sliding mode controller and the three controllers

A sliding mode controller with the sgn function replaced by the sat function is (see section 3)

$$\delta_f = -\frac{1}{b_0(x)}\left(f_0(x) - \ddot{y}_{sd} + \lambda\dot{e} + (\beta + k)\text{sat}(S/\phi)\right), \tag{96}$$

where $\ddot{y}_{sd}$ is the desired output and e is the tracking error, $e = y_s - y_{sd}$. For the vehicle lateral control problems, the desired output is zero in the road coordinate system, i.e., $y_{sd} = 0$.

It is pointed out in section 7 that the nonlinear term $f_0(x)$ can be splitted into two parts as

$$f_0(x) = f(x) - V_x\dot{\varepsilon}_d. \tag{97}$$

Then the sliding mode control law given by Eq. (96) can be rewritten as

$$\delta_f = -\frac{f(x)}{b_0(x)} + \frac{1}{b_0(x)} V_x \dot{\varepsilon}_d + \frac{1}{b_0(x)} \lambda \dot{y}_s - \frac{1}{b_0(x)} (\beta + k) \text{sat}(S/\phi). \tag{98}$$

For the lateral control of heavy vehicles, the desired output is zero, i.e., $y_{sd} = 0$; the vehicle articulation angle ε_f is very small at highway operations and $b_0(x)$ is a function of ε_f only, and thus, it may be approximated by a constant. So, when the sliding variable is within the boundary layer, i.e., $S \leq \phi$, Eq. (98) can be approximated by

$$\begin{aligned} \delta_f &= -\frac{f(x)}{b_0} + \frac{1}{b_0} V_x \dot{\varepsilon}_d - \frac{1}{b_0} \left(\lambda + \frac{\beta + k}{\phi} \right) \dot{y}_s - \frac{\lambda}{b_0} \frac{\beta + k}{\phi} y_s \\ &= -\frac{f(x)}{b_0} + \frac{1}{b_0} V_x \dot{\varepsilon}_d - k_1 \dot{y}_s - k_1 \lambda y_s. \end{aligned} \tag{99}$$

In Eq. (99), the last two terms represent linear feedback control, the PD control; the second term represents feedforward compensation whose magnitude is proportional to the centrifugal force; and the first term is nonlinear and represents all the modeled dynamics of the vehicle lateral control system including the Coriolis terms as well as terms contributed by the linear tire model. Apparently, the sliding mode controller is more involved than linear controllers. It consists of three parts: linear feedback control terms, a feedforward compensation term and a nonlinear feedback linearization term. In this section, we compare the following three controllers by experiments.

A. Linear controller,

$$\delta_f = -k_1 \dot{y}_s - k_1 \lambda y_s; \tag{100}$$

B. Linear controller with a fixed gain feedforward compensator,

$$\delta_f = \frac{1}{b_0} V_x \dot{\varepsilon}_d - k_1 \dot{y}_s - k_1 \lambda y_s; \tag{101}$$

C. Sliding mode controller given by Eq. (99).

The relationships among these three controllers are: controller B is obtained from controller A by adding a fixed gain feedforward compensation term and controller C is

Figure 17: Experimental Vehicle: Tractor-Semitrailer Combination

obtained from controller B by adding a nonlinear term which represents the modeled dynamics of the plant.

8.2 Test vehicle and instrumentation

The experimental vehicle shown in Fig. 17 is a combination of a Freightliner FLD 120 class 8 tractor and a Great Dane semitrailer, completed with a custom designed steering actuator, engine-throttle actuator, brake actuator, and on-board sensors. The sensors and actuators for the lateral and longitudinal control are as shown in Fig. 18.

Steering actuator: The steering actuator is developed by the NSK Corporation of Japan and it is mounted on the steering column. A robust inner-loop controller is designed for the sub-system represented by the input–output pair, input to the NSK motor driver–steering column angle (studied under MOU 313 and reported in California PATH Working Paper UCB-ITS-PWP-2000-1). A front wheel steering angle sensor is installed on the pitman arm, the output of the hydraulic power assist

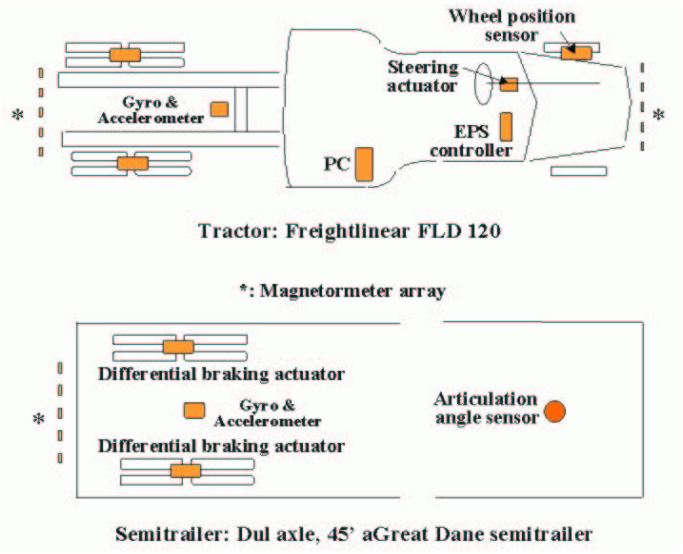

Figure 18: Sensors and Actuators for the Lateral and Longitudinal Control (*: Magnetometer Arrays)

unit of the steering system.

Brake actuator: The vehicle is installed with brake actuators with electronic control units as shown in Figs. 19 and 20. The electronic unit controls the pressure in the brake chambers. A brake chamber diaphragm is connected to an "S" cam by linkages such that an increase of pressure in the brake chamber pushes the brake shoe against the brake drum via the "S" cam and other linkages. At present, only the trailer brake actuators have the left and right independent braking capability which can be utilized in the lateral controller designs to stabilize the trailer yaw dynamics.

Lateral error sensors: PATH adopted a road-reference system based on magnetic markers. The primary sensors for the lane guidance are the magnetometers. On each of the front end of the tractor, the rear end of the tractor, and the rear end of the semitrailer, there is an array of magnetometers. Each magnetometer array has five magnetometers (see Fig. 21) that allow for a sensing range of $0.8m$ on either side of the road centerline along which magnets are buried in every $1.2m$. An algorithm is designed to obtain the lateral error at the middle sensor location with respect to

Figure 19: Brake Actuator

Figure 20: Brake Actuator: Air Pressure Transducer

Figure 21: Lateral Position Sensor: Magetometer Array

the road centerline from the signals of the magnetometers in an array.

Other sensors: Secondary/subsidiary sensors are also installed either for the controller synthesis or for the fault detection or for the safety and passenger comfort monitoring. They include:

- accelerometers: one on each of the tractor and semitrailer,
- gyroscopes: one on each of the tractor and semitrailer,
- wheel angle sensor: on the pitman arm, the output shaft of the hydraulic power assist unit of the steering system, and
- articulation angle sensor: around the fifth-wheel.

Hardware interface: A personal computer in the driver cabin of the tractor is in charge of communicating with sensors and actuators through National Instruments' DAQ board. The software for the real time implementation of controllers is based on the previous PATH software architecture and is suitably modified to accommodate new sensors and actuators. The QNX realtime operating system is used.

8.3 Open-Loop test and system parameter estimation

Open-loop tests were conducted to estimate some system parameters and verify the linear dynamic model given by Eq. (93). The experiments were conducted at Crows Landing. The test track is about $2000m$ long consisting of 3 curved sections and two straight sections at the beginning and at the end. As we previously pointed out, the linear vehicle model is a Linear Time Varying system (LPV) due to the appearance of the vehicle longitudinal velocity V_x in the system coefficients. To obtain the frequency response of the vehicle lateral dynamics, the frequency sweep tests are conducted at the velocities of $20mph$, $40mph$ and $60mph$. The steering actuator is given a sinusoidal reference command ranging in frequencies from $0.1Hz$ to $2.5Hz$. The recorded output signals are the lateral accelerations and the yaw rates of the tractor and the semitrailer, the articulation angle and the front steering wheel angle.

The system parameters are obtained as follows. Measured dimensional parameters are the distance between tractor's front wheel axle and rear wheel axle ($l_{f1} + l_{r1} = 5.35m$), the distance from tractor's rear axle to the fifth-wheel ($l_{r1} - d_{r1} = 3.67$) and the distance from the fifth-wheel to the semitrailer's rear axle ($d_{f2} + l_{r2} = 10.22m$). The inertia parameters are provided by the manufacturer: the mass of the tractor ($m_1 = 7956Kg$) and the mass of the empty semitrailer ($5682Kg$). The semitrailer is loaded with $5000Kg$ of concretes at the front end, therefore, the total mass of the semitrailer is $m_2 = 10682Kg$. Based on some heavy vehicle design specifications and guidelines, the location of the center of gravity of the tractor and that of the semitrailer are estimated. From the estimation and the dimensional measurements, we have $l_{f1} = 1.68m$, $l_{r1} = 3.67m$, $d_{r1} = 3.56m$, $l_{r2} = 7.32m$ and $d_{f2} = 2.90m$. The rest of the parameters such as the moment of inertia of the tractor (I^1_{zz}) and semitrailer (I^2_{zz}), the tire cornering stiffness ($C_{\alpha f}$, $C_{\alpha r}$ and $C_{\alpha t}$) and the location of the accelerometer on the tractor from the estimated c.g. of the tractor (d_s) are estimated by comparing the frequency response of the linear model at the velocities of $20mph$,

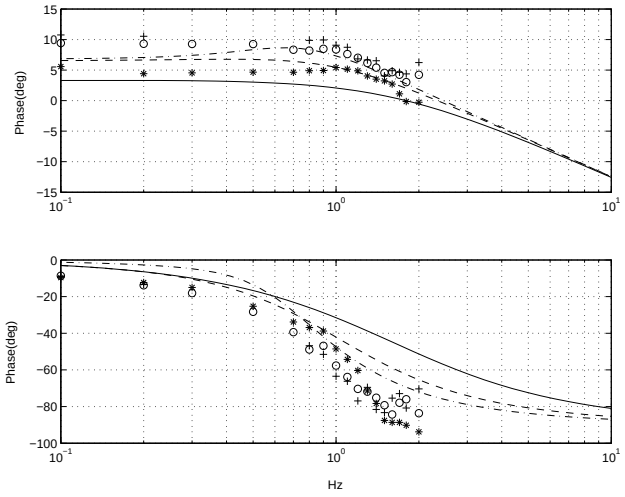

Figure 22: Frequency Response of the Tractor-Semitrailer System from the Steering Wheel to the Yaw Rate of the Tractor; Lines: Model; Marks: Experiments; $20mph$: Solid and *; $40mph$: Dashed and o; $60mph$: Dash-Dot and +

$40mph$ and $60mph$ with that of the experimental data at the corresponding velocities. The estimated parameters are as follows: $I^1_{zz} = 32000Kg \cdot m^2$, $I^2_{zz} = 482790Kg \cdot m^2$, $\mu = 0.75$, $C_{\alpha f} = \mu * 236904N/rad$, $C_{\alpha r} = \mu * 947618N/rad$, $C_{\alpha r} = \mu * 947618N/rad$ and $d_s = -1m$.

As shown in Figs. 22–25, the model, with the above system parameters, matches pretty closely the experimental frequency responses from the steering input to the yaw rate of the tractor, the yaw rate of the semitrailer, the acceleration at the tractor's accelerometer and the articulation angle. These provide us with confidence in designing model based controllers. The experimental data deviates from the linear model at higher frequencies due to the unmodeled dynamics of the road-tire interaction and the suspension system, among others.

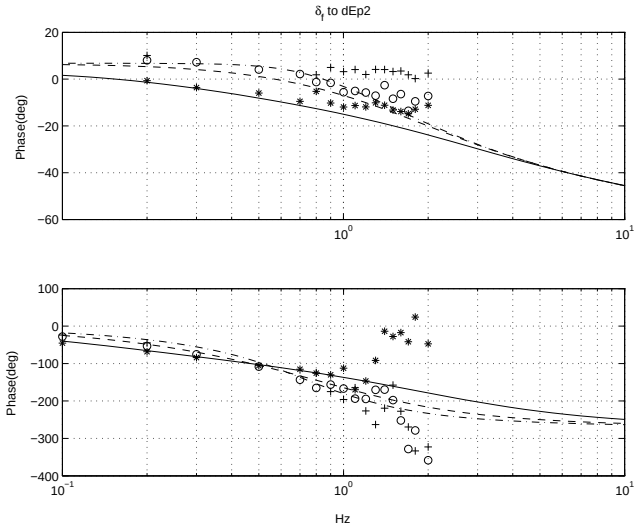

Figure 23: Frequency Response of the Tractor-Semitrailer System from the Steering Wheel to the Yaw Rate of the Semitrailer; Lines: Model; Marks: Experiments; $20mph$: Solid and *; $40mph$: Dashed and o; $60mph$: Dash-Dot and +

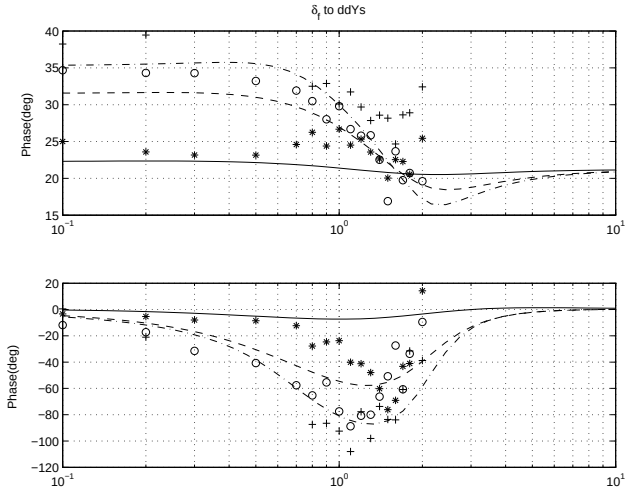

Figure 24: Frequency Response of the Tractor-Semitrailer System from the Steering Wheel to Acceleration of at the Front Bumper; Lines: Model; Marks: Experiments; $20mph$: Solid and *; $40mph$: Dashed and o; $60mph$: Dash-Dot and +

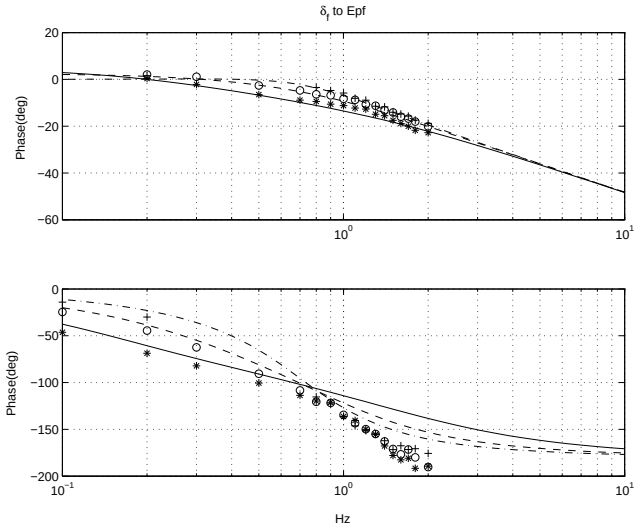

Figure 25: Frequency Response of the Tractor-Semitrailer System from the Steering Wheel to the Articulation Angle; Lines: Model; Marks: Experiments; $20mph$: Solid and *; $40mph$: Dashed and o; $60mph$: Dash-Dot and +

8.4 Closed-loop test and comparison of three controllers

In this section, we first describe some implementation issues of controllers and then present the experimental results of the three different controllers.

8.4.1 Implementation issues

As we can see from the vehicle model and the sensors installed, not all the system state variables are measurable. The unmeasured state variables have to be synthesized, estimated or observed from the sensor measurements.

Controller A needs two variables: y_s and $\dot{y}_s$. The system output y_s is given by Eq. (11) where y_r and ε_r are obtained from the front and rear magnetometer measurements based on the geometry [26]. $\dot{y}_s$ is obtained by numerically differentiating y_s.

In addition to the variables that controller A uses, controller B needs two more variables: V_x and $\dot{\varepsilon}_d$. The vehicle longitudinal speed V_x is measured and $\dot{\varepsilon}_d$ is obtained

from the equation

$$\dot{\varepsilon}_d = \dot{\varepsilon}_1 - \dot{\varepsilon}_r \tag{102}$$

where the tractor yaw rate $\dot{\varepsilon}_1$ is measured by gyro installed on the tractor and $\dot{\varepsilon}_r$ is obtained by numerically differentiating ε_r. The accuracy of this approach is readily verified from the experimental data as explained in subsection 8.4.2.

Nonlinear control algorithms such as controller C depend on the lateral errors measured at the front and rear ends of the tractor as well as many other sensors primarily for the computation of the feedback linearization term.

While feedback linearization is a sound analytical idea, the computation of the necessary terms requires many state variables which must be measured or estimated. Controller C needs 4 more variables than controller B: V_y, ε_1, ε_f and $\dot{\varepsilon}_f$. The tractor yaw rate $\dot{\varepsilon}_1$ and the articulation angle ε_f are measured. The articulation angle rate, $\dot{\varepsilon}_f$, is obtained from

$$\dot{\varepsilon}_f = \dot{\varepsilon}_2 - \dot{\varepsilon}_1, \tag{103}$$

where the yaw rates of the tractor and the semitrailer, $\dot{\varepsilon}_1$ and $\dot{\varepsilon}_2$, are measured. As for the estimation of the lateral velocity of the tractor's center of gravity, V_y, the lateral error measurements may be fused with the output of the lateral accelerometer, but it is not very satisfactory due to the bias and high noise level in the acceleration signal. However, noticing the relation,

$$\dot{y}_s = V_y + \varepsilon_r V_x + d_s \dot{\varepsilon}_r, \tag{104}$$

we can estimated tractor's lateral velocity from Eq. (104) as

$$V_y = \dot{y}_s - \varepsilon_r V_x - d_s \dot{\varepsilon}_r, \tag{105}$$

where all the signals on the right hand side of the equation can be obtained as explained in above.

Besides, all the signals but the magnetometer measurements at the front and rear bumper of the tractor are filtered using lowpass filters. While the lateral error

measurements by magnetometers are inherently intermittent, they are least contaminated by measurement noise, which is one of reasons that the implementation of linear control algorithms has been relatively easy compared to that of nonlinear control algorithms.

8.4.2 Experimental results

The major control objectives in vehicle lateral control are to maintain small lateral errors and to ensure passenger comfort. While there are not many passengers on tractor-semitrailer vehicles, the lateral acceleration and jerk must remain at reasonable levels. In robust nonlinear control algorithms, there is no explicit method of incorporating controller performance into the controller design. The smoothness of the steering input is one of the most important aspects from the viewpoint of public acceptance of automated driving. Most passengers do not like oscillatory steering motions even when it does not adversely affect the lateral acceleration and jerk. Thus, the final tuning of controller parameters must be performed by experiments. Selection of these parameters requires a good understanding of vehicle dynamics, control objectives, and limitations of the actuators.

The test track at Crows Landing consists of three curved sections extended by two straight sections. The radii of the curved sections are $800m$. Figures 26–31 show the experimental results of controllers A, B and C. The data were collected on the same day to ensure the same experimental environments such as the road condition, the vehicle condition the wind disturbance.

During experiments, the vehicle longitudinal velocity, V_x, was controlled by the driver. In Figs. 26, 28 and 30, plots (a)–(f) show the vehicle longitudinal speed V_x, the estimated yaw rate $\dot{\varepsilon}_d$, the steering angle command at the handwheel (δ_f) which is the output of the controller, the lateral tracking error at the tractor's front bumper y_{s1} (solid line) and rear bumper y_{s2} (dashed line), the yaw rate of the tractor $\dot{\varepsilon}_1$ and the orientation of the tractor in the road coordinate system ε_r, respectively.

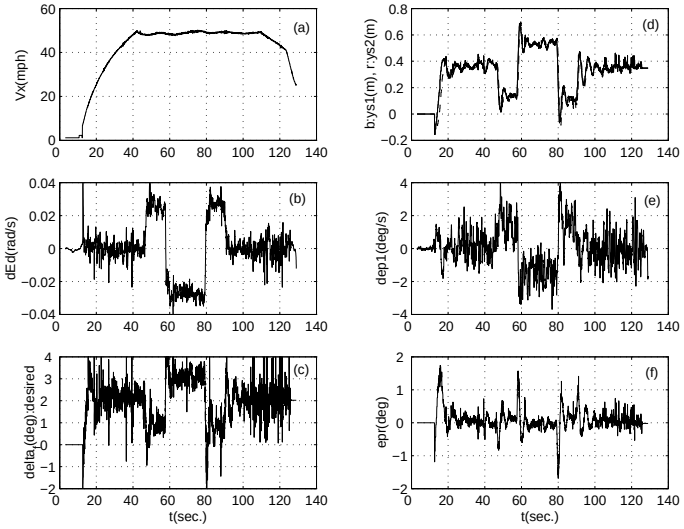

Figure 26: Experimental results of Controller A (1)

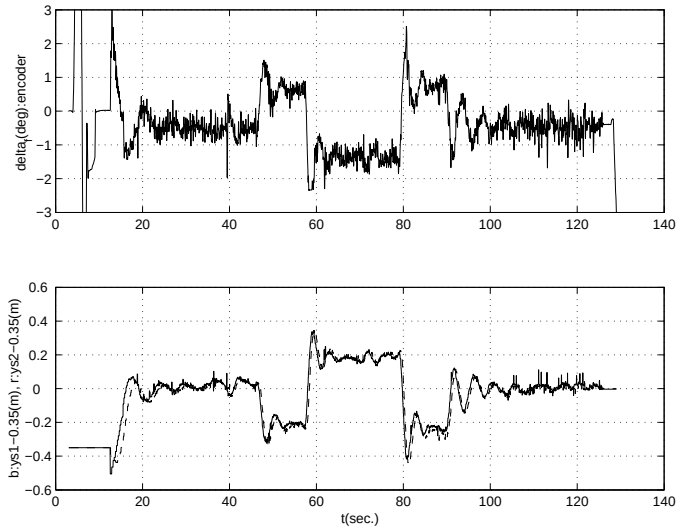

Figure 27: Experimental results of Controller A (2)

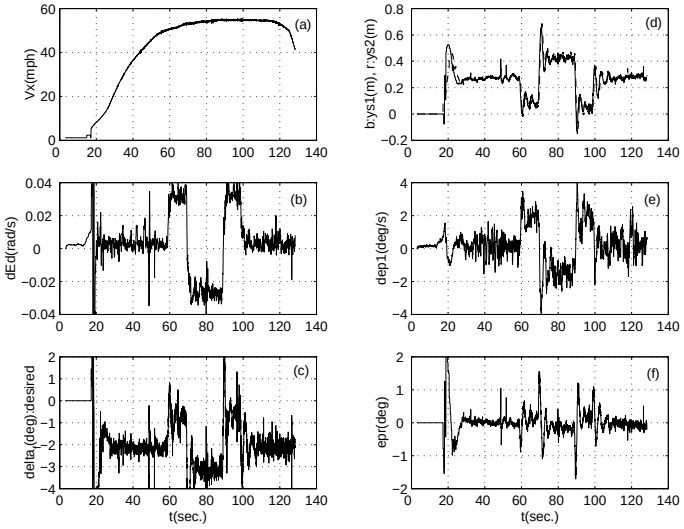

Figure 28: Experimental results of Controller B (1)

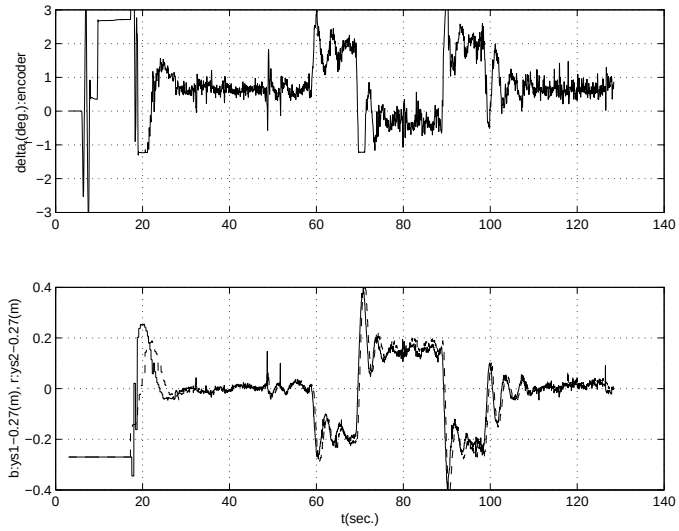

Figure 29: Experimental results of Controller B (2)

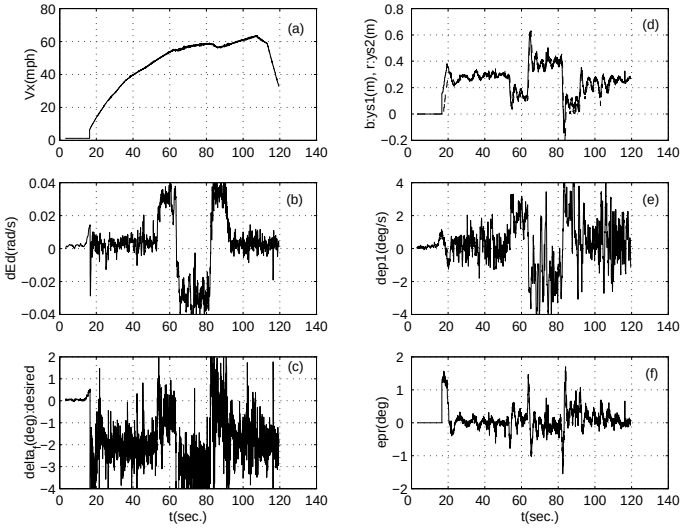

Figure 30: Experimental results of Controller C (1)

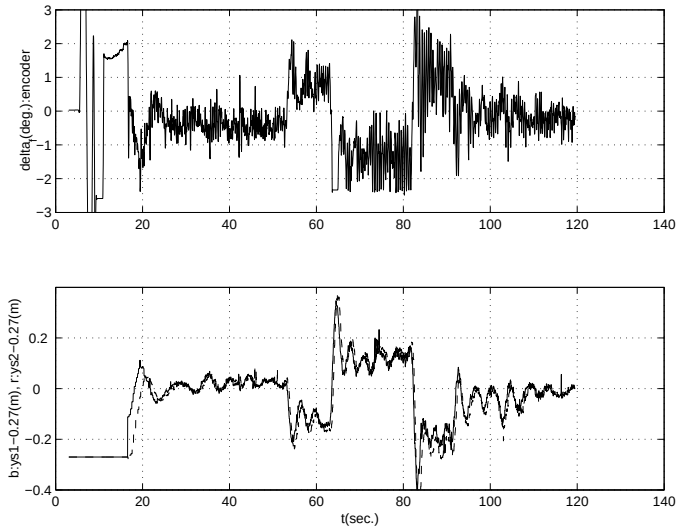

Figure 31: Experimental results of Controller C (2)

In the experiments with controller A, the vehicle longitudinal speed at the curved section was about $49mph$. Noting that the radius of the curve was $800m$, the desired yaw rate was about $0.027rad/s$. The estimated desired yaw rate in plot (b) of Fig. 26 is very close to this value, which verifies our estimation method.

In plot (c)'s of Figs. 26, 28 and 30, at the initial stage when $V_x = 0mph$, there is a large steering action. This is because, when we switch to the automatic driving mode, the inner-loop controller calibrates the front steering wheel to the "zero" position, i.e., the straight driving position, before turning on the lateral controller, and for the inner-loop controller to calibrate the steering wheel, the driver is asked to manually give a large steering angle to let the front steering wheel to pass through the "zero" position. In plot (d)'s of Figs. 26, 28 and 30, the lateral tracking error at the front and rear bumpers at the straight sections are nonzero. This is because, the current calibration algorithm is unreliable and often finds a wrong "zero" position. Whenever this happens, the steering command has to maintain a nonzero value at the straight road to let the front steering wheel point the actual "zero" position. The nonzero steering command is achieved by forcing the vehicle to have a nonzero lateral tracking error. Therefore, had the calibration algorithm found the correct "zero" position, the "ideal case", the actual tracking error should have been the data shown by the plot (d)'s minus the steady state tracking error at the straight sections as shown in the lower plots of Figs. 27, 29 and 31. In the following, whenever we say a lateral tracking error, we refer to the "ideal" case.

The upper plots of Figs. 27, 29 and 31 show the steering action of the steering column relative to the alleged "zero" position measured by the encoder.

With controller A, the maximum velocity we could reach was about $50mph$. It is linear and is very sensitive to the control parameters. Furthermore, the parameter range for which the controller can stabilize the vehicle lateral control system is rather small. In other words, the controller A is simple but not robust.

With controller B, the linear controller with a feedforward compensation, the max-

imum velocity we could reach while maintaining a reasonable performance such as small oscillation was bout $55mph$. It was not as sensitive as controller A to the controller parameters. Furthermore, controller B shows improved steady state tracking error ($16cm$) at the curved sections than controller A ($20cm$).

Controller C, the sliding mode controller, was tested at speeds as high as $60mph$ without letting the vehicle go unstable or go out of the magnetometer measurement range. For the data shown in Fig. 31, the steady state lateral tracking error is about $12cm$, the best among the three controllers.

9 Conclusions

In this report, we present lateral control, both control algorithm design and implementation, of heavy vehicle systems in the context of the automated highway systems. The major accomplishments of this research are summarized below.

Advanced robust control: To quantify lateral tracking error, a road coordinate system is defined, and to model the system output mimicing a human driver, a two-sensor scheme is introduced. The output dynamics is given in the road coordinate system.

Five controllers, a sliding mode controller, an adaptive robust controller, a nonlinear robust feedback linearization controller, a nonlinear loop-shaping controller and a linear robust feedback controller with a feedforward compensation, are designed and different controllers are compared by simulations whenever possible.

The sliding mode controller provides the basic robust stability. However, as the model uncertainty increases, the performance of the closed-loop system degrades dramatically. In the presence of parametric uncertainties in addition to the dynamical model uncertainties, the adaptive robust controller, by taking advantages of both robust and adaptive control techniques while overcoming their shortcomings, effectively lowers the control gain and improves the system performance.

we presented a new nonlinear robust controller for lateral control of tractor-semitrailer heavy vehicles. The new approach is to directly synthesize the robustness term based on a quadratic Lyapunov function. The control law resembled the ultimate bounded control approach. It was compared with another nonlinear robust controller based on sliding mode control. The design of robust nonlinear controllers was based on the Lyapunov's stability theorem and therefore they were robustly stable controllers. In either approach, feedback linearizaiton played a key role. The robust performances are usually achieved by fine tuning of controller parameters by simulations or experiments. The structure of the RFLC controller, however, suggests that there is a possibility of optimally choosing controller parameters in the design stage.

The nonlinear robust controller based on feedback linearization (RFLC) directly synthesizes the robustness term based on a quadratic Lyapunov function and it resembles the sliding mode controller. They are, however, fundamentally different in the ways of achieving robust stability. The two controllers are compared in the terms of their structure, the working principles and relative ease of tuning control parameters by simulations. In either approach, feedback linearizaiton played a key role. The robust performances are usually achieved by fine tuning of controller parameters by simulations or experiments. The structure of the RFLC controller, however, suggests that there is a possibility of optimally choosing controller parameters in the design stage.

By explicitly taking into account the steering subsystem dynamics and dynamically extending the systems to reduce chattering and prevent saturation in the front steering wheel, a robust controller is designed based on backstepping and modified robust control design approach. Simulation results show the effectiveness of the proposed controller in neutralizing the high control gain nature of robust controllers and improving the closed-loop performance.

An analogy between the vehicle lateral control system and a mechanical system

with a Coulomb friction is identified. Motivated by the friction compensation practices for the latter, feedforward compensators, a fixed again one and an adaptive one, are designed to enhance the linear feedback controllers in achieving a better tracking without sacrificing other performances. It is also pointed out that the nonlinear controllers actually involve the feedforward compensator corresponding to the fixed gain case. It is concluded that a linear robust feedback controller with a feedforward compensation of the road disturbance is a mid-point in terms of ease of implementation and control performances.

Implementation. It is shown that the sliding mode controller consists of three parts, linear feedback control term, a feedforward compensation term and a nonlinear feedback linearization term, and experimentally compared three controllers, a linear controller (controller A), a linear controller with a feedforward compensation (controller B) and a sliding mode controller (controller C). The comparison of experimental results of controller A and B not only verifies the results of section 7 that the feedforward compensation term in the feedback controller improve steady state tracking error without sacrificing system performance, but also shows that the feedforward compensation lifts the performance limit of the linear feedback controller and improves performance robustness to the control parameters. It is also shown that the sliding mode controller may provide as good performance as linear controllers.

It is, however, noted that the implementation of nonlinear controllers such as a sliding mode controller are much more complicated than that of linear controllers. Therefore, we conclude that the linear feedback controller with a feedforward compensation is a middle point between linear controllers and nonlinear controllers in terms of ease of implementation and control system performance, among the three controllers compared in this study. Finally, we note that the performance under linear control may be significantly improved by introducing more terms for better loop-shaping.

Acknowledgement

This work was sponsored by California PATH program. The contents of this report reflect the views of the authors who are responsible for the facts and the accuracy of the data presented herein. The contents do not necessary reflect the official views or policies of the states of California. This report does not constitute a standard, specification, or regulation. We also acknowledge the technical contributions of Dr. H.-S. Tan, D. Nelson, P. Krets, and W.-B. Zhang.

References

[1] H. Al-Deek and A. Kanafani. *Some Theoretical Aspects of the Benefits of en-Route Vehicle Guidance*. Tech. Rep. UCB-ITS-89-2, Institute of Transportation Studies, Univ. of California, Berkeley, 1989.

[2] H. Al-Deek, M. Martello, A. May, and W. Sanders. *Potential Benefits of in-Vehicle Information Systems in a Real Freeway Corridor under Recurring and Incident Induced Congestion*. Tech. Rep. UCB-ITS-PRR-88-2, Institute of Transportation Studies, Univ. of California, Berkeley, 1988.

[3] H. Al-Deek and A. May. *Potential Bebefits of in-Vehicle Information Systems (IVIS): Demand and Incident Sensitivity Analysis*. Tech. Rep. UCB-ITS-89-1, Institute of Transportation Studies, Univ. of California, Berkeley, 1989.

[4] de D. Bruin. *Lateral Guidance of All-Wheel Steered Multiple-Articulated Vehicles*. PhD thesis, Eindhoven Unniversit of Technology, the Netherlands, 2001.

[5] C. Chen and M. Tomizuka. Dynamic modelling of articulated vehicle for automated highway systems. In *Proceedings of American Control Conference*, pages 653–657, Evanston, IL, 1995.

[6] C. Chen and M. Tomizuka. Steering and braking control of tractor-semitrailer vehicles in automated highway systems. In *Proceedings of American Control Conference*, pages 658–662, Evanston, IL, 1995.

[7] C. Chen and M. Tomizuka. Steering and independent braking control for tractor-semitrailer vehicles in automated highway systems. In *Proceedings of the 34th IEEE Conference on Decision and Control*, pages 1561–1566, New York, NY, 1995.

[8] M. Corless and G. Leitmann. Continuous state feedback guaranteeing uniform ultimate boundedness for uncertain dynamic systems. *IEEE Transactions on Automatic Control*, 26(5):1139–1144, 1981.

[9] R. Fenton, G. Melocik, and K. Olson. On steering of automated vehicles: Theory and experiments. *IEEE Transactions on Automatic Control*, 21(3):306–315, 1976.

[10] R. Galijan, J. Gilkey, and R. Turner. System architecture and test results of a carrier phase gps-based lateral and longitudinal autoated highway system. In *Proceedings of the First World Congress on Applications of Transport Telematics and Intellignet Vehicle-Highway Systems*, pages 127–134, Paris, France, 1994.

[11] K. Gardels. *Automatic Car Controls for Electronic Highways.* Rep. GMR-276, General Motors Res. Lab., General Motors Corp., Warren, MI, 1960.

[12] P. Hingwe, A. Packard, and M. Tomizuka. Lpv controller for lateral control of heavy vehicles. In *Proceedings of American Control Conference*, Chicago, IL, 2000.

[13] N. Hounsell, M. McDonald, and L. Breheret. The modeling of dynamic route guidance. In *Advanced Telematics in Road Guidance*, pages 89–98, New York, 1989.

[14] A. Isidori. *Nonlinear Control Systems*. 1995.

[15] D. Jeffrey. Route guidance and in-vehicle information systems. In *Inf. Tech. Appl. Trans.*, P. Bonsall and M. Bell, Eds., Utrecht, Netherlands: VNU Science Press, 1987.

[16] U. Karaaslan, Pl Varaiya, and J. Walrand. Two proposals to improve freeway traffic flow. In *Prof. Ameri. Contr. Conf.*, pages 2539–2544, Boston, MA, 1991.

[17] F. Kobayashi. Feasibility study of route guidance. *Trans. Res. Rec.*, 737(107-112), 1979.

[18] M. Krstic, I. Kanellakopoulos, and P. Kokotovic. *Nonlinear and Adaptive Control Design*. Wiley, New York, 1995.

[19] H. Kusunoki, N. Komoda, M. Nakamura, R. Goudy, Y. Yasui, Y. Suzuki, M. Nakamura, and A. Arai. Vehicle lateral control development using laser radar to detect reflective lane markers. *Vehicle System Dynamics*, 25:359–369, 1996.

[20] R. Mahrt. Principles of automatic guidance of vehicles on a lane by means of permanent magnetic nails and board conmputer control. In *Proceedings of 21st IEEE Annual Conference on Vehicle Technology*, 1971.

[21] M. Nakamura, A. Arai, M. Bendett, M. Nakamura, R. Goudy, Y. Suzuki, and H. Kusunoki. Vehicle lateral control systes using laser radar. In *Proceedings of the SPIE-The International Society for Optical Engineering, Vol. 2344*, pages 267–277, 1995.

[22] S. Patwardhan, H. Tan, and J. Guldner. A general framework for automatic steering control: System analysis. In *Proceedings of American Control Conference*, pages 1598–1602, Alburquerque, New Mexico, 1997.

[23] K. Redmill. A simple vision system for lane keeping. In *Proceedings of Conference on Intelligent Transportation Systems*, pages 9–12, Boston, MA, 1997.

[24] S. Smulders. *Control of Freeway Traffic Flow*. Tech. Rep. OS-R8806, Center for Mathematics and Computer Science, Amsterdam, 1988.

[25] J. Sparmann. Lisb route guidance and information system: First results of the field trial. In *Prov. Vehicle Bav. Inf. Syst. Conf.*, pages 11–12, Toronto, Canada, 1989.

[26] M. Tai and M. Tomizuka. Robust lateral control of heavy vehicle for ahs. In *Proceedings of the the 14th IFAC World Congress, Vol. Q,*, pages 37–42, 1999.

[27] A. Teel. Adaptive tracking with robust stability. In *Proceedings of Conference on Decision and Control*, pages 570–575, 1993.

[28] P. Varaiya. Smart cars on smart roads: Problems of control. *IEEE Transactions on Automatic Control*, 38(2):195–207, 1993.

[29] J. Wang and M. Tomizuka. Analysis and controller design based on liner model for heavy-duty vehicles. In *International Mechanical Engineering Congress and Exposition, ASME Symposium on Transportation Systems*, pages 729–735, Anaheim, CA, 1998.

[30] J. Wang and M. Tomizuka. Robust H_∞ lateral control of heavy-duty vehicles in the automated highway system. In *Proceedings of American Control Conference*, 1999.

[31] J. Wang and M. Tomizuka. Coordinated steering and differential braking control for tractor-semitrailer combination vehicles. In *International Mechanical Engineering Congress and Exposition*, Orlando, FL, 2000.

[32] J. Wang and M. Tomizuka. Gain-scheduled h_∞ loop-shaping controller for automated guidance of tractor-semitrailer combination vehicles. In *Proceedings of American Control Conference*, pages 2033–2037, Chicago, IL, 2000.

[33] B. Yao. *Adaptive Robust Control of Nonlinear Systems with Application to Control of Mechanical Systems.* PhD thesis, Universty of California at Berkeley, Berkeley, CA, 1996.

[34] B. Yao and M. Tomizuka. Smooth robust adaptive sliding mode control of robot manipulators with guaranteed transient performance. In *Proceedings of American Control Conference*, pages 1176–1180, 1994.

[35] W. Zhang, R. Parsons, and T. West. An intelligent roadway reference system for vehicle lateral guidance/control. In *Proceedings of American Control Conference*, pages 281–286, 1990.

A Nonlinear Control Model of a Tractor-Semitrailer Vehicle System in the Vehicle Coordinate System

The control model of a tractor-semitrailer vehicle in the vehicle coordinate system is given by

$$M(q)\ddot{q} + c(q, \dot{q}, V_x) = 2C_{\alpha f}(1, l_{f1}, 0)^T \delta_f \tag{106}$$

where $q = (\int V_y, \varepsilon_1, \varepsilon_f)^T$,

$$M(q) = \begin{pmatrix} m_1 + m_2 & -m_2(d_{r1} + d_{f2}\cos\varepsilon_f) & -m_2 d_{f2}\cos\varepsilon_f \\ -m_2(d_{r1} + d_{f2}\cos\varepsilon_f) & I_{zz}^1 + I_{zz}^2 + m_2(d_{r1}^2 + d_{f2}^2) + 2m_2 d_{r1} d_{f2}\cos\varepsilon_f & I_{zz}^2 + m_2 d_{f2}^2 + m_2 d_{r1} d_{f2} \\ -m_2 d_{f2}\cos\varepsilon_f & I_{zz}^2 + m_2 d_{f2}^2 + m_2 d_{r1} d_{f2} & I_{zz}^2 + m_2 d_{f2}^2 \end{pmatrix} \tag{107}$$

$$
\begin{aligned}
c_1(q,\dot{q},V_x) = {} & (m_1+m_2)V_x\dot{\varepsilon}_1 + m_2 d_{f2}(\dot{\varepsilon}_1+\dot{\varepsilon}_f)^2\sin\varepsilon_f \\
& + \frac{2}{V_x}(C_{\alpha f}+C_{\alpha r}+C_{\alpha t})V_y + \frac{2}{V_x}(l_{f1}C_{\alpha f} - l_{r1}C_{\alpha r} - (d_{r1}+d_{f2}+l_{r2})C_{\alpha t})\dot{\varepsilon}_1 \\
& - \frac{2}{V_x}(d_{f2}+l_{r2})\dot{\varepsilon}_f - 2C_{\alpha t}\varepsilon_f
\end{aligned} \tag{108}
$$

$$
\begin{aligned}
c_2(q,\dot{q},V_x) = {} & -m_2(d_{r1}+d_{f2}\cos\varepsilon_f)V_x\dot{\varepsilon}_1 - m_2 d_{f2}V_y\dot{\varepsilon}_1\sin\varepsilon_f - 2m_2 d_{r1}d_{f2}\dot{\varepsilon}_1\dot{\varepsilon}_f\sin\varepsilon_f - m_2 d_{r1}d_{f2}\dot{\varepsilon}_1^2\sin\varepsilon_f \\
& + \frac{2}{V_x}(l_{f1}C_{\alpha f} - l_{r_1}C_{\alpha r} - (d_{r1}+d_{f2}+l_{r2})C_{\alpha t})V_y + \frac{2}{V_x}(l_{f1}^2C_{\alpha f} + l_{r1}^2C_{\alpha r} + (d_{r1}+d_{f2}+l_{r2})^2C_{\alpha t})\dot{\varepsilon}_1 \\
& + \frac{2}{V_x}(d_{f2}+l_{r2})(d_{r1}+d_{f2}+r_{r2})C_{\alpha t}\dot{\varepsilon}_f + 2(d_{r1}+d_{f2}+l_{r2})C_{\alpha t}\varepsilon_f
\end{aligned} \tag{109}
$$

$$
\begin{aligned}
c_3(q,\dot{q},V_x) = {} & -m_2 d_{f2}V_y\dot{\varepsilon}_1\sin\varepsilon_f - m_2 d_{f2}V_x\dot{\varepsilon}_1\cos\varepsilon_f + m_2 d_{r1}d_{f2}\dot{\varepsilon}_1^2\sin\varepsilon_f \\
& - \frac{2}{V_x}(d_{f2}+l_{r2})C_{\alpha t}V_y + \frac{2}{V_x}(d_{f2}+l_{r2})(d_{r1}+d_{f2}+l_{r2})C_{\alpha t}\dot{\varepsilon}_1 \\
& + \frac{2}{V_x}(d_{f2}+l_{r2})^2C_{\alpha t}\dot{\varepsilon}_f + 2(d_{f2}+l_{r2})C_{\alpha t}\varepsilon_f
\end{aligned} \tag{110}
$$

with $c = (c_1, c_2, c_3)^T$.

B Linear Model of a Tractor-Semitrailer Vehicle System in the Road Coordinate System

The linear model of a tractor-semitrailer in the road coordinate system is given by

$$
M_r\ddot{q}_r + D_r\dot{q}_r + K_r q_r = F_r\delta_f + E_1\dot{\varepsilon}_d(t) + E_2\ddot{\varepsilon}_d(t) \tag{111}
$$

where $q_r = (y_r, \varepsilon_r, \varepsilon_f)^T$,

$$
M_r = \begin{pmatrix}
m_1+m_2 & -m_2(d_{r1}+d_{f2}) & -m_2 d_{f2} \\
-m_2(d_{r1}+d_{f2}) & I_{zz}^1 + I_{zz}^2 + m_2(d_{r1}+d_{f2})^2 & I_{zz}^2 + m_2 d_{f2}^2 + m_2 d_{r1}d_{f2} \\
-m_2 d_{f2} & I_{zz}^2 + m_2 d_{f2}^2 + m_2 d_{r1}d_{f2} & I_{zz}^2 + m_2 d_{f2}^2
\end{pmatrix} \tag{112}
$$

$$
\begin{aligned}
D_r(1,1) &= \frac{2}{V_x}(C_{\alpha f} + C_{\alpha r} + C_{\alpha t}) \\
D_r(1,2) &= \frac{2}{V_x}(l_{f1}C_{\alpha f} - l_{r1}C_{\alpha r} - (d_{r1} + d_{f2} + l_{r2})C_{\alpha t}) + (m_1 + m_2)V_x \\
D_r(1,3) &= -\frac{2}{V_x}(d_{f2} + l_{r2})C_{\alpha f} \\
D_r(2,1) &= \frac{2}{V_x}(l_{f1}C_{\alpha f} - l_{r1}C_{\alpha r} - (d_{r1} + d_{f2} + l_{r2})C_{\alpha t}) \\
D_r(2,2) &= \frac{2}{V_x}(l_{f1}^2C_{\alpha f} + l_{r1}^2C_{\alpha r} + (d_{r1} + d_{f2} + l_{r2})^2)C_{\alpha t} - m_2(d_{r1} + d_{f2})V_x \\
D_r(2,3) &= \frac{2}{V_x}(d_{f_2} + l_{r2})(d_{r1} + d_{f2} + l_{r2})C_{\alpha t} \\
D_r(3,1) &= -\frac{2}{V_x}(d_{r2} + l_{r2})C_{\alpha t} \\
D_r(3,2) &= \frac{2}{V_x}(d_{f_2} + l_{r2})(d_{r1} + d_{f2} + l_{r2})C_{\alpha t} - m_2 d_{f2}V_x \\
D_r(3,3) &= \frac{2}{V_x}(d_{f2} + l_{r2})^2C_{\alpha t}
\end{aligned}
\tag{113}
$$

$$
K_r = \begin{pmatrix}
0 & -2(C_{\alpha f} + C_{\alpha r} + C_{\alpha t}) & -2C_{\alpha t} \\
0 & -2(l_{f1}C_{\alpha f} - l_{r1}C_{\alpha r} - (d_{r1} + d_{f2} + l_{r2})C_{\alpha t}) & 2(d_{r1} + d_{f2} + l_{r2})C_{\alpha t} \\
0 & 2(d_{f2} + l_{r2})C_{\alpha t} & 2(d_{f2} + l_{r2})C_{\alpha t}
\end{pmatrix}
\tag{114}
$$

$$
F_r = \begin{pmatrix}
2C_{\alpha f} \\
2C_{\alpha f}l_{f1} \\
0
\end{pmatrix}
\tag{115}
$$

$$
E_1 = \begin{pmatrix}
-\frac{2}{V_x}(l_{f1}C_{\alpha f} - l_{r1}C_{\alpha r} - (d_{r1} + d_{f2} + l_{r2})C_{\alpha t}) - (m_1 + m_2)V_x \\
-\frac{2}{V_x}(l_{f1}^2C_{\alpha f} + l_{r1}^2C_{\alpha r} + (d_{r1} + d_{f2} + l_{r2})^2)C_{\alpha t} + m_2(d_{r1} + d_{f2})V_x \\
-\frac{2}{V_x}(d_{f_2} + l_{r2})(d_{r1} + d_{f2} + l_{r2})C_{\alpha t} + m_2 d_{f2}V_x
\end{pmatrix}
\tag{116}
$$

$$E_2 = \begin{pmatrix} m_2(d_{r1} + d_{f2}) \\ -(I_{zz}^1 + I_{zz}^2 + m_2(d_{r1} + d_{f2})^2) \\ -(I_{zz}^2 + m_2 d_{f2}^2 + m_2 d_{r1} d_{f2}) \end{pmatrix} \tag{117}$$